



**Scalable Nanomanufacturing of Inkjet-Printed Wearable  
Energy Storage Devices**

Journal:	<i>Journal of Materials Chemistry A</i>
Manuscript ID	TA-REV-05-2019-005239.R2
Article Type:	Review Article
Date Submitted by the Author:	26-Jun-2019
Complete List of Authors:	Huang, Tao-Tse; Purdue University Wu, Wenzhuo; Purdue University, School of Industrial Engineering

SCHOLARONE™  
Manuscripts

## Scalable Nanomanufacturing of Inkjet-Printed Wearable Energy Storage Devices

Tao-Tse Huang<sup>1</sup>, Wenzhuo Wu<sup>1, 2\*</sup>

<sup>1</sup>School of Industrial Engineering, Purdue University, West Lafayette, Indiana 47907, USA

<sup>2</sup>Flex Laboratory, Purdue University, West Lafayette, Indiana 47907, USA

\*Author to whom correspondence should be addressed.

Email: W. Z. W. ([wenzhuowu@purdue.edu](mailto:wenzhuowu@purdue.edu))

### Abstract

The economic production and integration of nanomaterials-based wearable energy storage devices with mechanically-compliant form factors and reliable performance will usher in exciting opportunities in emerging technologies such as consumer electronics, pervasive computing, human-machine interface, robotics, and the Internet of Things. Despite the increased interests and efforts in nanotechnology-enabled flexible energy storage devices, reducing the manufacturing and integration costs while continuously improving the performance at the device and system level remains a major technological challenge. The inkjet printing process has emerged as a potential economic method for nanomanufacturing printed electronics, sensors, and energy devices. Nevertheless, there have been few reports reviewing the scalable nanomanufacturing of inkjet printed wearable energy storage devices. To fill this gap, here we review the recent advances in inkjet printed flexible energy storage technologies. We will provide an in-depth discussion focusing on the materials, manufacturing process integration, and performance issues in designing and implementing the inkjet printing of wearable energy storage devices. We have also compiled a comprehensive list of the reported device technologies with the corresponding processing factors and performance metrics. Finally, we will discuss the challenges and opportunities associated with related topics. The rapid and exciting progress achieved in many emerging and traditional disciplines are expected to lead to more theoretical and experimental advances that would ultimately enable the scalable nanomanufacturing of inkjet printed wearable energy storage devices.

**Keywords:** inkjet printing, wearable energy storage devices, supercapacitors, batteries, nanomaterials

## 1. Introduction

The economic production and integration of nanomaterials-based wearable energy storage devices with mechanically-compliant form factors and reliable performance will provide exciting opportunities in emerging technologies such as consumer electronics, pervasive computing, human-machine interface, robotics, and the Internet of Things (IoT)<sup>1-10</sup>. Lithium-ion batteries (LIBs) are the most widely used commercial portable energy storage devices, with a projected global market value at 26 billion USD by 2023. Meanwhile, the supercapacitors market was estimated to be around 948.63 million USD in 2018 and is projected to have an annual growth of 18.69% from 2019 to 2024. Prototypes of flexible energy storage devices that exhibit lightweight and mechanical deformability have been recently developed in technology sectors with huge market needs, such as smart textiles, biomedical electronics, and implementable systems<sup>8, 11, 12</sup>. Several commercial electronic devices with folding and rolling capability, such as the Samsung Galaxy Fold and the LG flexible TV, were also introduced recently.

Despite the increased interests and efforts in nanotechnology-enabled flexible energy storage devices, reducing the manufacturing and integration costs while continuously improving the performance at the device and system level remains a major technological challenge. The inkjet printing process has emerged as a potential economic method for nanomanufacturing printed electronics, sensors, and energy devices, due to advantages such as full digital mask-less printability, versatile ink formulation, cost-effectiveness, low working temperature, and feasibility for scale-up production<sup>13-15</sup>. Many efforts have been devoted to developing the related technology, and several review articles provided good coverage discussing the material and process aspects of inkjet printed devices<sup>16, 17</sup>. Nevertheless, to our best knowledge, there have been few reports reviewing the scalable nanomanufacturing of inkjet printed wearable energy storage devices. To fill this gap, here we review the recent advances in inkjet printed flexible energy storage technologies. The recent rapid increase in the research interests and efforts in related areas can be seen in **Fig. 1**, which was generated by conducting a bibliometric analysis using the keywords of “nanomaterial” “inkjet printing” “flexible” and “energy storage device”. We will provide an in-depth discussion focusing on the materials and process integration. Finally, we will discuss the challenges and opportunities associated with the scalable nanomanufacturing of inkjet-printed wearable energy storage devices.

## 2. State-of-the-art flexible energy storage devices

The most commonly used electrochemical energy storage (EES) devices are batteries and supercapacitors (SCs). Various types of flexible batteries were reported in the literature, such as the lithium-ion battery<sup>18-26</sup>, zinc-air battery<sup>27-33</sup>, lithium-sulfur battery<sup>34-38</sup>, lithium-air battery<sup>39, 40</sup>, sodium ion battery<sup>41-46</sup>, and aluminum-air battery<sup>39, 47</sup>, among which flexible LIBs are the most widely researched and utilized. A detailed discussion of the recent developments in flexible batteries can be found in previous review papers<sup>8, 23, 48-51</sup>. The three types of supercapacitors are the electrochemical double layer capacitor, pseudocapacitor, and hybrid capacitor, which is the combination of the previous two<sup>52-54</sup>. The major difference between batteries and SCs is that batteries can store large amounts of energy while with relatively low power density, which leads to longer charge periods. Supercapacitors, on the other hand, possess high power densities with lower energy densities than those typical for batteries. A detailed review of the general principles

and recent progress in flexible supercapacitors could be found in Ref<sup>12, 55</sup>. Flexible EES usually consist of several components, including an anode, cathode, divider, electrolyte, and a current collector, which should all have bending capability and shape compatibility to achieve the overall flexibility of the device. Nanomaterials with high electrochemical performance are usually utilized as active materials, such as metal oxides<sup>52, 54, 56-60</sup>, conductive polymers<sup>61-69</sup>, carbon-based materials<sup>70-80</sup>, and other emerging materials, such as titanium carbide<sup>81-84</sup>. Various configurations of flexible EES have been provided in a review by Dubal et al<sup>55</sup> which are cable-type (**Fig. 2a**), sandwich (**Fig. 2b**), planar, wire-type (**Fig. 2c**)<sup>85</sup>, and fiber-shaped (**Fig. 2d**) structure<sup>86</sup>. This review primarily focuses on the inkjet printing of planar and sandwich-structured devices.

### 3. Process elements in inkjet printing for nanomanufacturing wearable energy devices

A recent review on advances in flexible EES devices by Wang et al. discussed numerous techniques for fabricating flexible EES. Conventional techniques such as spray deposition, chemical vapor deposition (CVD), electrochemical deposition, and sputtering have been widely employed for fabricating flexible EES devices<sup>87-92</sup>. However, the lack of process scalability and the convoluted processing conditions make these techniques unfavorable for large-scale manufacturing. Compared to the conventional fabrication methods, printing techniques, especially inkjet printing, presents a facile and effective process for manufacturing flexible EES due to the feasibility and flexibility of printing various individual components as well as the integrated systems at large-scale.

Dozens of manufacturing methods have been developed for printing EES devices<sup>93</sup>. The commonly utilized printing techniques for depositing nanomaterials include screen-printing, transfer printing, 3D printing, and inkjet printing<sup>94-96</sup>. The screen-printing technique deposits ink onto a substrate with the use of a pre-patterned mask. The transfer printing technique starts by patterning a material on a substrate, followed by transferring the printed materials to another substrate. 3D printing extrudes material out of the nozzle and deposits the material onto the substrate, where multi-layer printing is utilized for stacking the patterns into three-dimensional structures. The inkjet printing process hinges on an extrusion-based ink deposition, which ejects the suspension from the nozzle and deposits it onto the substrates (**Fig. 3**). The inkjet printing process can be categorized into continuous inkjet (CIJ) (**Fig. 3a**)<sup>97</sup> and drop-on-demand (DOD) (**Fig. 3b**)<sup>97</sup> methods. The CIJ method deposits a continuous stream of ink onto the substrates and recycles the excess ink, while the DOD method deposits discrete ink droplets at the predesigned locations which offer less contamination and cost-effective printing of precious materials. The two main types of inkjet printheads are thermal and piezoelectric, as shown in **Fig. 3b**. Thermal print heads contain a resistive heater inside the ink chamber for superheating the ink so that it can flow through the printhead. Piezoelectric printheads contain a mechanism that oscillates due to electrical excitation and purges the ink through the chamber by forming a pressure wave. Other than the thermal and piezoelectric printheads, an electrohydrodynamic printing technique was also discussed in the literature<sup>98-100</sup>. In all the inkjet printing processes, the droplet ejection is highly dependent on the viscosity, surface tension, and density of the ink. Benefits possessed by the inkjet printing process, specifically, the DOD method includes maskless, rapid deposition, scalability from small droplet to large area fabrication, less contamination, good material compatibility, less wastage, and low cost.

Some key processing elements for the inkjet printing include the dimensions of the nanomaterial, material agglomeration, ink concentration, droplet travel distances, ink viscosity, the surface tension of the ink, etc. The size of the material should be at least 50 times less than the printing nozzle for avoiding the To avoid clogging the nozzles<sup>94-96</sup>, which could be achieved through co-designing and controlling the synthesis and preparation of nanomaterials. The agglomeration of materials could be resolved by incorporating surfactants or dispersing agents, such as dimethylformamide (DMF)<sup>83, 101-104</sup>, N-methyl pyrrolidone (NMP)<sup>82, 105, 106</sup>, or propylene glycol<sup>13, 107</sup>. The concentration of the ink is also critical for the inkjet printing process, where a too high concentration can clog the nozzle and too low value can significantly increase the printing time for desired feature dimensions<sup>93, 108, 109</sup>. A small droplet traveled distance is ideal for the inkjet printing process with improved control of the feature dimensions and spatial locations. The idea ink viscosity should be around 1 to 20 cP<sup>82, 93, 109</sup>, which is significantly lower than that for screen-printing or 3D printing, and surface tension value should be below 80 N/m for efficient printing onto versatile substrates<sup>93, 109</sup>.

In addition to the above guidelines for inkjet printing in general, there are some specific requirements that need to be taken into consideration for inkjet printing of wearable EES. To ensure the quality of the printing process, the ink should meet the required viscosity and surface tension. The dimension of the nanomaterial should also be in an acceptable range, which is generally 50 times smaller than the size of the printhead, to avoid the clogging of the nozzles. To ensure the quality of the printed film and the device performance, annealing or film compression are usually utilized after the inkjet printing process. These post-printing processes need to be compatible with the printed materials, e.g., not causing material degradation, and should be well controlled to ensure the desired mechanical flexibility and robustness that are needed in the wearable EES applications. The long-term stability of the printed devices is critical for practical applications. Cyclic aging characterization is usually required for probing the material and device stability/reliability when the devices are subject to bending, deformation, elevated temperature, and humidity. Consequently, the selection of active materials, substrates, electrolyte, and current collector should all be put into consideration since these components need to have properties that are capable of creating devices that have not only good electrical performance but also desired mechanical robustness.

Current inkjet printing technology is capable of printing nanoparticles (NP) dispersions, conducting polymers, biological molecules, 1D and 2D nanostructures. Nanomaterials offer advantages over bulk material for enhanced electrochemical performance due to the lightweight, superior mechanical properties, high porosity, and large surface area. The performance of flexible batteries and flexible SCs is primarily determined by their electrode materials<sup>93, 109</sup>, which makes the selection of active material critical. Most of the materials utilized require incorporating other materials for the enhancement of physical durability and energy capacity<sup>11</sup>. In the following sections, we will review recent advances in inkjet printing flexible batteries and supercapacitors.

## **4. Inkjet printing of nanomaterials for wearable batteries**

### **4.1. Inkjet printed flexible zinc-air battery**

Hilder *et al*<sup>110</sup> demonstrated the fabrication of a flexible zinc-air battery using both the inkjet printing and screen-printing process. The anode was created utilizing screen-printing with a

combination of zinc/carbon/polymer composite. The poly(3,4-ethylene dioxythiophene) (PEDOT) cathode was prepared with inkjet printing a pattern of iron (III)p-toluenesulfonate ((FepTS)<sub>3</sub>) as a solution in 1-Butanol onto a paper. A solution of lithium chloride (LiCl)/lithium hydroxide (LiOH) was prepared as an electrolyte and inkjet printed onto the paper substrate. The authors compared the device performance with different processing conditions, such as different electrolytes, various Zn contents, the utilization of polyethylene naphthalate (PEN), and paper substrates. The result concluded that an 8 M LiCl electrolyte contributes to higher efficiency than the 1M NaCl does since the absence of water in the LiCl system leads to the reduction of aqueous zinc corrosion. Also, the devices with 1 M NaCl electrolyte showed no significant difference in efficiency when different Zn contents were used; while a significant enhancement in efficiency was observed under high Zn content for devices printed with 8 M LiCl electrolyte. The comparison between the substrates suggested that paper substrates led to less superior performance, possibly due to the highly porous substrate structure. The study provided important processing knowledge for inkjet printing flexible Zinc-air batteries, particularly on the selection of proper electrolyte and substrate, which suggests the utilization of high-molarity electrolytes and less-porous substrates can lead to improved device performance. Such fundamental knowledge can be applied in future studies for further optimization of the inkjet printed devices.

#### **4.2 Inkjet printed flexible zinc-silver battery**

Ho *et al*<sup>98</sup> reported an alkaline zinc-silver micro-battery with 3D pillar electrodes utilizing a super inkjet printing (SIJP) technique. Silver (Ag) nanopaste was mixed with n-tetradecane as the ink for printing the current collectors for both electrodes. The Ag current collector also served as the backbone structure for depositing the electroplated zinc onto the negative electrode and silver oxide on the positive electrode. An aqueous electrolyte solution of KOH with dissolved ZnO was used for the battery operation. The study suggested that the conductivity and the porosity of the printed structures were influenced by the temperature and duration of the post-printing sintering process. Moreover, the performance characterization showed that the 3D pillar electrodes possess an up to 60% increase in capacity compared to a planar electrode with the same footprint. The device was printed using an electrohydrodynamic actuator, which also significantly reduced the droplet volume and hence enabled better printing resolutions compared to that can be achieved by commercial printers with piezoelectric or thermal printheads. The electrohydrodynamic printing technique is capable of printing smaller feature size, can be utilized not only printing batteries but also for other electronic devices. The 3D pillar geometry can also be applied to other EES devices for performance enhancement.

#### **4.3 Inkjet printed flexible lithium-sulfur battery**

Sulfur as a cathode material has characteristics such as high specific capacity, non-toxic, and low cost, which are beneficial for producing cost-effective batteries. However, sulfur has poor cyclic performance and conductivity<sup>111</sup>, which necessitates the incorporation of conductive materials for improved battery performance. To address this issue, Milroy *et al*<sup>34</sup> reported the inkjet printing of a lithium-sulfur (Li-S) battery which utilized single-wall carbon nanotubes (SWNT) infused with electronically conductive sulfur straight-chain (S@SWNT) as the integrated current-collector/active-material composite. A post-printing annealing process was implemented to remove the excess solvent, where the printed structures were annealed on a hot plate with a

gradual increase of 4°C per minute from 25 to 150 °C, followed by heating at 150 °C for 10 to 15 minutes. The printed devices show a capacitance of 800 mAh/g initially and 700 mAh/g after 100 cycles, which is promising for potential applications in supplying power to thin-film devices. The study suggested that the gradual increase of annealing temperature at a suitable rate (e.g., 4°C per minute) is essential for preserving the shape conformality. On the contrary, an increased rate below 2°C per minute can lead to an inhomogeneous electrode due to the undesired Marangoni effect (**Fig. 4a**). Few studies have been performed on flexible Li-S batteries as well as the inkjet printing of such devices, likely due to the lack of understandings in the corresponding electrochemical processes. Further research is necessary to understand better the printing process and how it could engineer and affect the properties of the printed materials and structures in future wearable Li-S batteries with enhanced performance.

#### 4.4 Inkjet printed flexible Lithium-ion battery

Lithium iron phosphate (LiFePO<sub>4</sub>, LFP), one of the commonly used cathode materials for EES, offers unique characteristics such as high capacity, low cost, and is environmental benign<sup>111</sup>. Gu and colleagues<sup>19</sup> utilized the DOD inkjet printing method and water-soluble LFP for fabricating LIB cathodes, with aluminum (Al) foil and CNT micro-paper as the current collector. The authors found that the binding and interaction between the printed active materials and CNT paper leads to better electrochemical performance than the devices with Al current collectors. The study also provided interesting and important manufacturing knowledge regarding the effects of ink impurity and oxygen content in the LFP on the performance of the printed devices. The authors revealed that the impurities in the suspension would lower the electrical conductivity of LiFePO<sub>4</sub> and hence lead to higher resistance and significant energy loss. Moreover, the removal of oxygen content from water could prevent the oxidation of LiFePO<sub>4</sub> to Fe<sub>2</sub>O<sub>3</sub> and Fe<sub>3</sub>O<sub>4</sub>. Similar studies by Ben-Barak *et al*<sup>20</sup> and Delannoy *et al*<sup>112</sup> also demonstrated inkjet-printed LFP cathode for flexible LIBs using DOD printing method. LiCoO<sub>2</sub> is another cathode material with a high specific capacitance that has been utilized for printing LIBs. Huang *et al*<sup>113</sup> fabricated a thin-film LiCoO<sub>2</sub> electrode for LIB via inkjet printing and observed a 95% retention rate after 100 charge-discharge cycles. Their study also suggested that the device can be charged at various current densities, e.g., even as high as 384 μA/cm, without compromising the charge and discharge efficiency. It should be noted, though, LiCoO<sub>2</sub> suffers from the poor conductivity and high cost, which limit its manufacturing potential for printing cost-effective, flexible LIBs at large scale.

There have also been a few studies reporting the inkjet printing of anodes for LIBs using nanomaterials. Zhao *et al*<sup>114</sup> demonstrated the fabrication of tin oxide (SnO<sub>2</sub>) thin-film anode for rechargeable LIBs with a high discharge capacitance of 812.7 mAh/g through inkjet printing. For the preparation of the SnO<sub>2</sub> ink, wet ball-milling was used for stabilizing the SnO<sub>2</sub> NP and acetylene black (AB) with two polymeric hyperdispersants (CH10B and CH12B). The thickness of the SnO<sub>2</sub> thin film can be controlled by repeating the printing procedure on the Cu foil substrate, followed by direct compression of the printed-film for the subsequent electrochemical characterization. Zhao *et al*<sup>115</sup> presented a printed Li<sub>4</sub>Ti<sub>5</sub>O<sub>12</sub> (LTO) thin films on a gold (Au) substrate as the anode for LIBs. The excellent electrochemical properties of the device suggested the promise of ink-jet printing for manufacturing future flexible LIBs. In a separate study, Delannoy and colleagues<sup>116</sup> focused on the inkjet printing of sol-gel silica-based ionogel (**Fig. 4b**) as the solid electrolyte for LIBs, with LFP and LTO being the electrodes. This study is interesting

and unique in the sense that most other reported work focused on the inkjet printing of electrodes. A list of the reported inkjet-printed flexible battery devices is compiled in **Table 1**, and the performance of those devices is summarized in **Table 2**. The corresponding Ragone plots of the devices are shown in **Figs. 7a**, and **b**.

**Table 1.** Various components fabricated via inkjet printing in the literature.

Ref	Component	Material	Additives	Apparatus	Devices
110	Cathode Electrolyte	PEDOT LiCl/ LiOH	Pyridine, polyurethane diol PEG	DMP 2811, Dimatrix	Zinc-air battery
98	Electrode	silver nanopaste	n-tetradecane	Customized super inkjet printing	Zinc-silver battery
117	Electrode	75 wt % MnO <sub>2</sub>	25 wt% PVDF-HFP, THF, 2 M NH <sub>4</sub> Cl	Lexmark 3200	Manganese battery
34	Cathode	Sulfur infused SWNT-MET	CHP	DMP 2800, Dimatrix	Li-S battery
113	Cathode	LiCoO <sub>2</sub>	Lomar D, carbon black, monoethanolamine, NaCMC	Canon BJC- 1000sp printer	LIB
19	Cathode	LFP, carbon black, SCMC at 8:1:1	triton X-100, glycerin	DMP 2800, Dimatrix	LIB
20	Cathode	LFP, carbon black	DI water, Triton X-100, NaCMC	PICO Pμlse	LIB
114	Anode	SnO <sub>2</sub>	AB, hyperdispersant (CH10B, CH12B), DI water/absolute ethanol/diethylene glycol/triethanolamine/IPA 56: 18:5:1:1 by mass	Canon BJC- 1000sp	LIB
115	Anode	LTO	AB, hyperdispersant (CH10B, CH12B), DI water/absolute ethanol/diethylene glycol/triethanolamine/IPA 56: 18:5:1:1 by mass	Canon BJC- 1000sp	LIB
112	Electrode	LFP, carbon black	triton X 100, CMC, PAMA	Piezoelectric printer	LIB
116	Electrolyte	PYR13-Li-TFSI	N/A	DMP 2800, Dimatrix	LIB

108	Anode	MnO <sub>2</sub> , 200 mg MWCNT, 160 mg	200 mg SDBS, 40 ml DI water	HP Deskjet 1010 inkjet printer	SC
	Conductive pattern	Ag 200 mg MWCNT, 160 mg Ag	200 mg SDBS, 40 ml DI water		
118	Electrode	2 mg/ml GO	N/A	DMP 2800, Dimatix	SC
119	Electrode	2 mg/ml GO	N/A	DMP 2800, Dimatix	SC
120	Current collector Anode	Ag ink  K <sub>2</sub> CO <sub>3</sub> (P <sub>2</sub> O <sub>7</sub> ) <sub>2</sub> ·2H <sub>2</sub> O nanocrystal	dispersant: ethanol	DMP 3000, Dimatrix	MSC
	Cathode	graphene nanosheet			
121	Electrode	0.2 mg/ml SWNTs	1 wt% aqueous SDS in DI water	Epson Artisan 50 piezoelectric printer	SC
122	Electrode	AC	5% EG, PTFE, Triton-X 100	N/A	MSC
123	Electrode	200 mg NGP, 200 mg PANI	200 mg SDBS and 100 ml water	Piezoelectric printer	SC
124	Electrode	AC powder, SWNT	1.0 wt% SDBS	HP Deskjet 1010	SC
	Current collector	Ag NW	water/IPA in 1:1 (v/v)		
	Substrate	CNF suspension	N/A		
	Electrolyte	Li: ([BMIM][BF <sub>4</sub> ])	ETPTA, ethanol or water		
107	Electrode	δ-MnO <sub>2</sub> nanosheet, 3 - 4% PEDOT	TBA•OH, H <sub>2</sub> O <sub>2</sub> , Triton X-100, EG, propylene glycol/water in 1:10 (M/M)	DMP 2800, Dimatix	MSC
125	Electrode	GO 10 mg/ml	N/A	DMP 2800, Dimatix	SC
	Electrode	GH-PANI nanocomposite	Ammonia, H <sub>2</sub> SO <sub>4</sub> , water/ethanol in 1:1		
56	Cathode	AC	EG, NMP	EPSON L130	SC
	Substrate	GO	NMP		
	Anode	GO-MnO <sub>2</sub>	NMP		
	Electrode	MnO <sub>2</sub>	EG, NMP		
126	Electrode	Graphene, PEDOT: PSS	EG/PH1000, IPA	N/A	All-solid- state MSC

127	Electrode	PEDOT: PSS, Ag grid	Triton-X100, EG	DMP 3000, Dimatrix	Transparent SC
128	Tracks	PANI	DMSO, CSA, TFMS	Piezoelectric printer	Negative SC
101	Electrode	Graphene	Toluene, Ethyl cellulose, DMF, ethanol, terpineol	DMP 2800, Dimatrix	MSC
129	Electrode	Graphene nanosheet	Ethyl cellulose, terpineol/ethanol in 3:1 (v/v)	DMP 2800, Dimatrix	Transparent MSC
130	Electrode	MWCNT	IPA, ethanol, DMF, ODCB, chloroform, water	HP Deskjet D2360	SC
70	Electrode Electrolyte	Graphene IL: [EMIM][TFSI]	EC, ethanol, NaCl, EG PS-PMMA-PS, n-butyl acetate	MJ-AT-01, MicroFab	MSC
131	Electrode	rGO	DI water	N/A	SC
132	Electrode	GO/ Commercial pen ink 49:1 (v/v)	EG	DMP 2800, Dimatrix	MSC
133	Electrode	Graphene, ethyl cellulose	cyclohexanone, terpineol, di (ethylene glycol) methyl ether 80:15:5 v/v	Ceradrop X-Serie, DMC-11610	MSC
134	Electrode	PEDOT: PSS – CNT/Ag	N/A	DMP 2800, Dimatrix	MSC
82	Electrode	Ti3C2Tx MXene ink	NMP, DMSO	DMP 2800, Dimatrix	MSC
135	Electrode Electrolyte	Graphene PSSH	DMF, EC, toluene :ethanol 80:20 poly(4-styrenesulfonic acid), EG, phosphoric acid	DMP 2800, Dimatrix	MSC

**Note:** Multi-wall carbon nanotubes (MWCNT); single-walled carbon nanotube (SWNT); graphene oxide (GO); nano graphene platelets (NGP); polyaniline (PANI); Deionized water (DI water); sodium dodecyl sulfate (SDS); sodium dodecylbenzene sulfonate (SDBS); isopropylalcohol (IPA); ionic liquid (IL); polytetrafluoroethylene (PTFE); carboxymethyl cellulose (CMC); tetrahydrofuran (THF); ethylene glycol (EG); acetylene black (AB); carbon black (CB); activated carbon (AC); carbon nanofiber (CNF); LiFePO<sub>4</sub>(LFP) ; Li<sub>4</sub>Ti<sub>5</sub>O<sub>12</sub> (LTO); cumene hydroperoxide (CHP); N-Methylpyrrolidone (NMP); tetrabutylammonium hydroxide (TBA-OH); manganese dioxide (MnO<sub>2</sub>); 1-butyl-3-methylimidazolium tetrafluoroborate ([BMIM][BF<sub>4</sub>]); poly(3,4-ethylenedioxythiophene)(PEDOT); cellulose nanofibers (CNF); tin oxide (SnO<sub>2</sub>); lithium chloride (LiCl); lithium hydroxide (LiOH); polyethylene glycol (PEG), poly-acrylic-co-maleic acid (PAMA), N-methyl-N-propylpyrrolidinium bis(trifluoromethane) sulfonylimide ionic liquid (PYR13-TFSI); lithium bis(trifluoro-methane)sulfonylimide salt (Li-TFSI); ethoxylated trimethylolpropane triacrylate (ETPTA); dimethylsulfoxid (DMSO), S)-(+)-10-Camphorsulfonic acid (CSA). The table was recompiled based on the review paper by Zhang et al.<sup>136</sup> with additional information.

**Table 2.** Performance of various devices fabricated via inkjet printing.

Ref	Potential window	Capacitance	Max energy density	Max power density	Cycle stability	Mechanical stability	Devices
110	0 ~ 0.8 V	polyethylene naphthalate substrate 1.4 mA h cm <sup>-2</sup> paper-based 0.5 mA h cm <sup>-2</sup> (Sandwich) (Dimension N/A)	N/A	N/A	N/A	N/A	Zinc-air battery
98	1.1 ~ 2.0 V	N/A (3D) (9 mm <sup>2</sup> )	3.95 mW h cm <sup>-2</sup>	70 Wh Kg <sup>-1</sup>	N/A	N/A	Zinc-silver battery
117	-0.5 ~ 0.65 V	270 mA h g <sup>-1</sup> at 4.01 A g <sup>-1</sup> (N/A) (0.5 cm x 0.7 cm)	N/A	N/A	N/A	N/A	Manganese battery
34	1.6 ~ 2.8 V	800 mA h g <sup>-1</sup> at C/2 (Sandwich) (2mm x 2mm, 5mmx 5mm)	N/A	N/A	100 cycle 87.5% retention	N/A	Li-S battery
113	3.0 ~ 4.2 V	120 mA h g <sup>-1</sup> at 180 μA cm <sup>-2</sup> 132 mA h g <sup>-1</sup> at 64 μA cm <sup>-2</sup> 115 mA h g <sup>-1</sup> at 192 μA cm <sup>-2</sup> 105 mA h g <sup>-1</sup> at 394 μA cm <sup>-2</sup>	N/A	N/A	100 cycles 95% retention	N/A	LIB

		(Configuration N/A) (0.5 cm <sup>2</sup> )					
19	2.0 ~ 4.0 V	Al current collector 129.9 mA h g <sup>-1</sup> at 0.1 C CNT current collector 151.3 mA h g <sup>-1</sup> at 0.1 C (Coin-type with thin film electrodes) (Dimension N/A)	N/A	N/A	30 cycle ~100% retention	N/A	LIB
20	0 ~ 1.0 V	140 mA h g <sup>-1</sup> at 0.1 C 80 mA h g <sup>-1</sup> at 6 C (Coin-type with thin film electrodes) (12 mm diameter)	N/A	N/A	100 cycle 98.2% retention	N/A	LIB
114	0.05 ~ 1.2 V	812.7 mA h g <sup>-1</sup> at 33 μA cm <sup>-2</sup> (Coin-type with thin film electrodes) (1.5 cm <sup>2</sup> )	N/A	N/A	50 cycle 30.78%	N/A	LIB
115	1.0 ~ 2.0 V	174 mA h g <sup>-1</sup> at 10.4 μA cm <sup>-2</sup> (Configuration N/A; thin film electrode) (Dimension N/A)	N/A	N/A	300 cycle 88% retention	N/A	LIB
112	2.5 ~ 4.0 V	150 mA h g <sup>-1</sup> at 1C 125 mA h g <sup>-1</sup> at 9C ~90 mA h g <sup>-1</sup> at 18C <30 mA h g <sup>-1</sup> at 45C ~30 mA h g <sup>-1</sup> at 90C (Configuration N/A) (Dimension N/A)	N/A	N/A	100 cycle ~100% retention	N/A	LIB

116	2.0 ~ 4.1 V	60 mA h g <sup>-1</sup> at C/10 (3D) (10mm diameter, 1 mm thick)	N/A	N/A	100 cycle ~100% retention	N/A	LIB
108	0 ~ 1.8 V	Overall device N/A MnO <sub>2</sub> -Ag-MWCNT anode 30.5 F cm <sup>-3</sup> at 10 mV s <sup>-1</sup> MnO <sub>2</sub> -Ag-MWCNT anode 4.1 F cm <sup>-3</sup> at 1 V s <sup>-1</sup> Filtrated MWCNT cathode 5.3 F cm <sup>-3</sup> at 10 mV s <sup>-1</sup> (Sandwich) (1.5 cm x 1 cm)	1.28 mW h cm <sup>-3</sup>	512.1 mW cm <sup>-3</sup>	3000 cycles 96.9% retention	Bending to curvature of 10, 20, 30, and 40%, with a maximum change in electrical resistance of 25%. Bending at 20% curvature over 2000 cycles with less than 10% change in electrical resistance	SC
118	0 ~ 1 V	0.5 M H <sub>2</sub> SO <sub>4</sub> electrolyte 124 F g <sup>-1</sup> at 20 mV s <sup>-1</sup>	2.6 W h kg <sup>-1</sup>	5.8 kW kg <sup>-1</sup>	500 cycle ~65% retention	Bending 350 cycles led to less than 5% capacitance	SC
	0 ~ 1 V	1 M H <sub>2</sub> SO <sub>4</sub> electrolyte 192 F g <sup>-1</sup> at 20 mV s <sup>-1</sup>	5 W h kg <sup>-1</sup>	10 kW kg <sup>-1</sup>			
	0 ~ 3 V	BMIM BF <sub>4</sub> electrolyte 73 F g <sup>-1</sup> at 20 mV s <sup>-1</sup> (Sandwich) (3 cm x 3 cm)	5.5 W h kg <sup>-1</sup>	19 kW kg <sup>-1</sup>			
119	-0.6 ~ 0.4 V	Device 125 F g <sup>-1</sup> at 50 mV s <sup>-1</sup> Device 132 F g <sup>-1</sup> at 0.01 V s <sup>-1</sup> Device 48 F g <sup>-1</sup> at 0.5 V s <sup>-1</sup> (Configuration N/A) (Dimension N/A)	6.74 W h kg <sup>-1</sup>	2.19 kW kg <sup>-1</sup>	1000 cycle 96.8% retention	N/A	SC
120	0 ~ 0.6 V	6.0 F cm <sup>-3</sup> at 10 mA cm <sup>-3</sup>	0.96 mW h cm <sup>-3</sup>	54.5 mW cm <sup>-3</sup>	5000 cycle	Bending from 0 – 180	MSC

		(Planar) (Dimension N/A)			94.4% retention	degree with negligible change in performance	
121	0 ~ 1.0 V	Overall 138 F g <sup>-1</sup> SWNT-PET electrode 65 F g <sup>-1</sup> SWNT-fabric electrode 60 F g <sup>-1</sup> (Sandwich) (6 cm <sup>2</sup> )	18.8 W h/kg 8.2 W h/kg 6.1 W h/kg	96 kW kg <sup>-1</sup> 4.5 kW kg <sup>-1</sup> 3.0 kW kg <sup>-1</sup>	1000 cycle ~100% retention	N/A	SC
122	0 ~ 2.5 V	2.1 mF cm <sup>-2</sup> (Planar) (1.5mm x 1mm)	N/A	44.9 mW cm <sup>-2</sup>	N/A	N/A	MSC
123	0 ~ 1.0 V	NGP/PANI 82 F g <sup>-1</sup> 1 NGP 10 F g <sup>-1</sup> (Sandwich) (Dimension N/A)	2.4 W h kg <sup>-1</sup> 1 0.3 W h kg <sup>-1</sup> 1	124 kW kg <sup>-1</sup> 132 kW kg <sup>-1</sup>	1000 cycle 85.7% retention 1000 cycle 100% retention	N/A	SC
124	0 ~ 2.0 V	100 mF cm <sup>-2</sup> (Planar) (2 cm x 3 cm)	N/A	N/A	10000 cycle ~100% retention	Bending hundreds of cycles at radius 1, 3, and 5 mm with negligible change in performance	SC
107	0 ~ 0.8 V	2.4 F cm <sup>-3</sup> at 0.05 A cm <sup>-3</sup> (Planar) (dimension N/A)	1.8x10 <sup>-4</sup> W h cm <sup>-3</sup>	0.018 W cm <sup>-3</sup>	3600 cycle 88% retention	Bending at 120 degree (radius 1 cm) for 250 cycles, small crack occurs	Solid-state MSC
125	0 ~ 0.8 V	864 F g <sup>-1</sup> at 1A g <sup>-1</sup> (3D) (dimension N/A)	24.02 W h kg <sup>-1</sup>	3202.4 W kg <sup>-1</sup>	1000 cycle 96% retention	Bending at 45, 90, and 180 degree with 1% decrease in capacitance, less than 2% decrease in capacitance after 100 bending	SC

						cycle at 180 degree	
56	0 ~ 2.0 V	1023 F g <sup>-1</sup> at 4 mA cm <sup>2</sup> (sandwich) (dimension N/A)	22 mW h cm <sup>-3</sup>	0.4 W cm <sup>-3</sup>	9000 cycle 89.6% retention	Bending from 0 – 360 degree with negligible change in performance, 98.4% retention rate after bending at radius 6 mm over 1000 cycles	SC
126	0 ~ 1.0 V	5.4 mF cm <sup>-2</sup> at 1 mV s <sup>-1</sup> 2 mF cm <sup>-2</sup> at 5 mV s <sup>-1</sup> (Planar) (2 cm x 3 cm)	N/A	N/A	5000 cycle 90 % retention	Bending over 1000 cycles with negligible change in performance	All-solid-state MSC
127	0 ~ 0.8 V	PEDOT: PSS SC 1.18 mF cm <sup>-2</sup> PEDOT: PSS electrode 4.72 mF cm <sup>-2</sup> PEDOT: PSS/Ag SC 1.84 mF cm <sup>-2</sup> PEDOT: PSS/Ag electrode 7.36 mF cm <sup>-2</sup> (Sandwich) (2 cm x 2 cm)	0.38 mW h cm <sup>-2</sup>	0.036 W cm <sup>-2</sup>	5000 cycle 83.7 % retention	Bending from 0, 60, 120, and 180 degree with negligible change in performance, however, electrical resistance increases as repeated deformation is present	Transparent SC
128	N/A	-799 F g <sup>-1</sup> (Configuration N/A) (Dimension N/A)	N/A	N/A	N/A	N/A	Negative SC
101	-0.4 ~ 0.4 V	0.82 mF cm <sup>-2</sup> at 10 mV s <sup>-1</sup> 0.19 mF cm <sup>-2</sup> at 100 mV s <sup>-1</sup> (Planar) (Dimension N/A)	N/A	8.8 mW cm <sup>-2</sup>	N/A	N/A	MSC
129	0 ~ 1.0 V	71% light transmittance 99 μF cm <sup>-2</sup>	N/A	N/A	10,000 cycle 91.3 % retention	Bending at radius 7.5 and 5 cm with negligible	Transparent MSC

		90% light transmittance 16 $\mu\text{F cm}^{-2}$ (Planar) (2 cm x 3.5 cm)				change in performance, a 93.1 retention rate at the bending radius of 2.75 cm	
130	-0.5 ~ 1.5 V	ACN+TBAP 268 $\pm$ 12 F/g	4.5 $\pm$ 0.2 Wh $\text{kg}^{-1}$	2 $\pm$ 0.09 kW $\text{kg}^{-1}$	1000 cycle 90 % retention	N/A	SC
	0 ~ 1.0 V	H <sub>2</sub> SO <sub>4</sub> 240 $\pm$ 10 F/g	29.7 $\pm$ 1.2 Wh $\text{kg}^{-1}$	1.1 $\pm$ 0.05 kW $\text{g}^{-1}$	1000 cycle 92 % retention		
	-0.2 ~ 1.0 V	Na <sub>2</sub> SO <sub>4</sub> 233 $\pm$ 9 F/g	6.2 $\pm$ 0.2 Wh $\text{kg}^{-1}$	1.2 $\pm$ 0.05 kW $\text{kg}^{-1}$	1000 cycle 87 % retention		
	0 ~ 0.5 V	KOH 120 $\pm$ 11 F/g (Configuration N/A) (Dimension N/A)	0.22 $\pm$ 0.02 Wh $\text{kg}^{-1}$	0.3 $\pm$ 0.03 kW $\text{kg}^{-1}$	1000 cycle 85 % retention		
70	0 ~ 1.0 V	268 $\mu\text{F cm}^{-2}$ at 10 mV $\text{s}^{-1}$ (Planar) (2.22 mm x 0.46 mm)	N/A	N/A	1000 cycle 97% retention	Bending at radius of 1 cm over 1000 cycles with negligible change in performance	MSC
131	0 ~ 3.5 V	EMIMBF <sub>4</sub> 0.63 F $\text{cm}^{-3}$ , 39 F/g	1.06 mW h $\text{cm}^{-3}$ , 63 Wh $\text{kg}^{-1}$	0.408 W/ $\text{cm}^3$ , 25.5 kW $\text{kg}^{-1}$	N/A	Bending from 0 – 180 degree with negligible change in performance	SC
	0 ~ 2.75 V	TEABF <sub>4</sub> 0.82 F $\text{cm}^{-3}$ , 51 F/g	0.87 mW h $\text{cm}^{-3}$ , 54.2 Wh $\text{kg}^{-1}$	0.259 W/ $\text{cm}^3$ , 16.2 kW $\text{kg}^{-1}$			
	0 ~ 1 V	H <sub>2</sub> SO <sub>4</sub> 0.70 F $\text{cm}^{-3}$ , 43 F/g (Planar) (1.75 mm x 1.89 mm)	0.09 mW h $\text{cm}^{-3}$ , 6 Wh $\text{kg}^{-1}$	0.089 W/ $\text{cm}^3$ , 5.6 kW $\text{kg}^{-1}$			
132	0 ~ 0.8 V	19 $\mu\text{F cm}^{-2}$ (Planar) (1 cm x 1 cm)	N/A	N/A	10,000 cycles 100% retention	Bending at 90 degree for 500 cycles with negligible change in performance	MSC

133	0 ~ 1.0 V	Full device 17.8 F cm <sup>-3</sup> at 0.25 A cm <sup>-3</sup> Electrode 71.2 F cm <sup>-3</sup> at 0.5 A cm <sup>-3</sup> (Sandwich) (2.6 cm x 0.9 cm)	2.47 mW h cm <sup>-3</sup>	40.3 W cm <sup>-3</sup>	10,000 cycles 100% retention	Bending at radius 2.5 mm for 5000 cycles with negligible change in performance, bending strain of 2.5 %	MSC
134	0 ~ 0.9 V	23.6 F cm <sup>-3</sup> (Planar) (1.2 cm <sup>2</sup> )	42.1 mW h cm <sup>-3</sup>	89.1 mW cm <sup>-3</sup>	10,000 cycles 92% retention	Bending from 0 – 90 degree with negligible change in performance	MSC
82	0 ~ 0.5 V	562 F cm <sup>-3</sup> (Planar) (4 mm x 8 mm)	0.32 μW h cm <sup>-2</sup>	158 μW cm <sup>-2</sup>	10,000 cycles 100% retention	Bending for 0 -150 degree over 1000 cycles with negligible change in performance, slight decrease in conductivity at 150 degree	MSC
135	0 ~ 1.0 V	0.7 mF cm <sup>-2</sup> (Planar) (4 mm x 8 mm)	1 mW h cm <sup>-3</sup>	0.1 W cm <sup>-3</sup>	11,000 cycles 77% retention	N/A	MSC

### 5 Inkjet printing of nanomaterials for flexible supercapacitors

Due to the unique characteristics such as low cost, high conductivity, porous structure, and excellent electrochemical stability, carbon-based materials, such as activated carbons (ACs), carbon nanotubes (CNTs), and graphene are the typical electrode materials for EDLCs<sup>11, 19</sup>. It should be noted that specific surfactants are needed for printing carbon-based material since most of these materials are not hydrophilic. For CNTs, sodium dodecyl sulfate (SDS) and sodium dodecyl benzene sulfonate (SDBS) is the typically dispersing agents<sup>136</sup>. Metal oxides and conductive polymers are the primary materials for printing pseudocapacitors. For instance, manganese dioxide (MnO<sub>2</sub>), which has remarkable theoretical specific capacitance, natural abundance, low cost, and environment-friendliness, is one of the most investigated metal oxides for EES<sup>56, 107, 117, 130</sup>. Besides MnO<sub>2</sub>, ruthenium dioxide (RuO<sub>2</sub>) has also been primarily investigated for SCs<sup>121</sup>. Characteristics such as excellent energy storage capability make polyaniline (PANI) and polypyrrole (PPy) the two typical conducting polymers for SCs. PEDOT is the most studied

conducting polymer for flexible SCs due to its high conductivity and solution processability<sup>11</sup>. However, these conductive polymer fibers lack mechanical strength and long-term stability, necessitating the integration of these polymers with other more stable conductive materials.

### 5.1 Inkjet printed flexible electric double layer capacitor (EDLC)

Le *et al*<sup>119</sup> demonstrated the fabrication of a graphene supercapacitor electrode via DOD method, using a piezoelectric printhead with the utilization of thermal reduction of graphene oxide (GO). In a separate study, Ervin and colleagues<sup>118</sup> also reported the inkjet-printed flexible graphene-based SCs, where the electrodes were fabricated by inkjet printing GO ink onto the Kapton current collector. The authors identified the effects of the electrolytes, e.g., types and concentration, on the performance of printed SC devices. They revealed that printed devices using 1 M K<sub>2</sub>SO<sub>4</sub> showed the highest capacitance, and the devices using ionic liquid BMIM BF<sub>4</sub> exhibited the highest energy and power density. Ervin and colleagues also investigated the impacts of the annealing temperature on the device performance and found that a high annealing temperature could lead to enhanced capacitance in the printed devices. This study further provided valuable manufacturing knowledge for improving the performance of printed SC devices. Hyun *et al*<sup>70</sup> presented a unique fabrication technique that deposited graphene ink onto a UV-curable polymer molding, followed by a photonic annealing process utilizing an intense pulsed lamp (IPL) (**Fig. 5a**). The authors studied the effects of the various widths of the printed interdigital electrodes on the SC performance and concluded that the increased finger width would lead to improved performance. Hyun and colleagues further evaluated the manufacturability of their process by investigating the operation of 44 printed devices, which showed little variation in the device performance. Li and colleagues<sup>133</sup> demonstrated a high-performance inkjet printed micro supercapacitor (MSC) using graphene ink. Various electrode thicknesses ranging from 30 to 2000 nm were investigated, and the result suggested that a printed electrode thickness of 40 nm led to the highest device performance. In another study, Pei *et al*<sup>132</sup> fabricated a hybrid ink by mixing GO ink and commercial pen ink for inkjet printing a solid-state MSC. Interestingly, the hybrid ink gave rise to a significant enhancement in the areal capacitance of the printed devices compared to the ones printed with pure GO ink. The study suggested that such improvement is likely due to the reduced ink agglomeration with the small amount addition of commercial pen ink.

Besides graphene, activated carbon (AC) is also widely used for inkjet printing EDLCs. Pech *et al*<sup>122</sup> developed a carbon-based micro SC for a self-powered module by inkjet printing AC ink onto a silicon substrate with an Au current collector (**Fig. 5b**). The ink consists of a mixture of AC powder, PTFE polymer binder, ethylene glycol (EG), and surfactant. A 1M Et<sub>4</sub>NBF<sub>4</sub> propylene carbonate serves as the electrolyte, giving rise to a wide potential range of 0 ~ 2.5 V with a cell capacitance of 2.1 mF/cm<sup>2</sup> for the printed device. Choi *et al*<sup>124</sup> demonstrated a fully printed device with multiple inkjet-printed components, including SWNT/AC as the active electrode materials, Ag nanowire ink for the current collector, cellulose nanofibril (CNF) suspension as the primer layer on the paper substrate, and solid-state [BMIM][BF<sub>4</sub>]/ETPTA electrolyte (**Fig. 5c**). The incorporation of Ag nanowire (NW) into the SWNT network led to a significant improvement in the electrical conductivity of the inkjet-printed electrode. The printed device also showed excellent mechanical flexibility, with no significant degradation in the structural integrity or

electrochemical performance after 1000 bending cycles. Ujjain *et al*<sup>130</sup> demonstrated the inkjet printing of highly conductive aromatic functionalized MWCNT for SC on flexible PET substrates. The authors performed a comprehensive investigation of various electrolytes and identified that ACN+TBAP electrolyte led to the largest capacitance and power density while H<sub>2</sub>SO<sub>4</sub> electrolyte gave rise to the highest energy density of the printed devices. These findings are significant since the ACN+TBAP electrolyte could provide an alternative option to the highly acidic electrolyte. Jung *et al*<sup>131</sup> presented a printed electrode using rGO ink and found that the ionic liquid EMIMBF<sub>4</sub> electrolyte led to the highest energy and power density, while the TEABF<sub>4</sub> electrolyte induced the highest capacitance.

### 5.2 Inkjet printed flexible pseudocapacitor

Pseudocapacitive materials, e.g., metal oxides, metal sulfides and conducting polymers, are promising electrode materials since their capacitance generally far exceeds the double-layer capacitance achievable with carbon materials<sup>137</sup>. The exploration of inkjet printed pseudocapacitor is still at its infancy. Wang *et al*<sup>107</sup> demonstrated a flexible solid-state MSC by inkjet printing  $\delta$ -MnO<sub>2</sub> nanosheets and PEDOT: PSS on a polyimide substrate. The authors explored the mitigation of the coffee-ring effect, a major issue occurring during the inkjet printing process, with the addition of propylene glycol. The printed pseudocapacitor device showed excellent mechanical flexibility with little degradation in the electrochemical performance after cyclic bending (**Fig. 5d**). The relationship between the thickness of the printed layer and the device performance was also examined. The result suggested that an optimal thickness existed for the device performance. Cheng *et al*<sup>127</sup> inkjet printed a transparent MSC using PEDOT: PSS/Ag grid as the active materials and compared the performance of the PEDOT: PSS/Ag and PEDOT: PSS electrodes. They found that the incorporation of Ag grid gave rise to the improved energy density, electrode capacitance, and overall device capacitance. Moreover, the flexible and transparent nature of the device also enhances the aesthetic appearance for better wearable experience with diversified functionality.

### 5.3 Inkjet printed flexible hybrid supercapacitor

A hybrid supercapacitor hybridizes the EDLCs and pseudocapacitors with the integration of carbon materials, conductive polymers, and metal oxides<sup>54, 138, 139</sup>. Hybrid capacitors can be further grouped into three subcategories, i.e., asymmetric capacitors, battery-type capacitors, and composite capacitors. Pang *et al*<sup>120</sup> reported a high performance flexible solid-state asymmetric micro-supercapacitor, which has the potential to be integrated into roll-up display panels and power-on-chip systems. The device was fabricated through inkjet printing the graphene nanosheet and lamellar K<sub>2</sub>Co<sub>3</sub>(P<sub>2</sub>O<sub>7</sub>)<sub>2</sub>·2H<sub>2</sub>O nanocrystal whiskers, which are eco-friendly materials and synthesized under mild hydrothermal conditions. The device showed a high specific capacitance 6.0 F/cm<sup>3</sup> with a high retention rate of 94.4% after 5000 cycles. The mechanical flexibility of the device was also evaluated, showing excellent deformability with large degree bending. Xu and colleagues<sup>123</sup> demonstrate the inkjet-printed electrodes using the graphene/polyaniline (PANI) ink, with 1 M H<sub>2</sub>SO<sub>4</sub> as the electrolyte. The graphene/PANI electrode showed excellent electrochemical performance and long cycle life. The authors also conducted a comparison between graphene/PANI and graphene electrodes, revealing that the presence of PANI led to a significantly improved energy density (2.4 W·h/kg) compared to the devices with

only graphene electrodes (0.3 W·h/kg). It should be noted, though, the graphene/PANI electrode resulted in a slightly decreased power density (124 kW/kg) compared to the case with graphene electrode (132 kW/kg). In a separate study, Chi *et al.*<sup>125</sup> demonstrated a fully inkjet-printed device using 3D porous graphene hydrogel/PANI nanocomposite with a gel electrolyte supported on graphene papers (**Fig. 5e**).

The inkjet printing of metal oxide nanomaterials has also been explored for fabricating flexible hybrid capacitors. Chen *et al.*<sup>121</sup> employed an inkjet-printed SWNT/RuO<sub>2</sub> nanowire (NW) thin-film electrode for flexible SCs, where the RuO<sub>2</sub> NWs were synthesized through a chemical vapor deposition (CVD) method. The authors found that the SWNT/PET devices had a superior performance in terms of the capacitance, energy density, and power density. Such findings have important implications for future industrial manufacturing of flexible SC devices. The results of this study also suggested that the incorporation of RuO<sub>2</sub> NW led to improved specific capacitance, power density, and energy density. Such understanding provides fundamental yet essential manufacturing knowledge such as the process-structure-property-performance relation for engineering the preparation of the materials and optimizing the inkjet printing process. Wang *et al.*<sup>108</sup> presented an asymmetric capacitor through inkjet printing MnO<sub>2</sub>-Ag-MWCNT composites into the anode. A filtrated MWCNT cathode was fabricated using a vacuum filtration method with the addition of SDBD surfactant. The fabricated devices exhibited high capacitance, energy density, power density, and retention rate. The incorporation of the highly conductive nanomaterials here, i.e., Ag nanoparticles and MWCNT, helps mitigate the poor electrical conductivity of MnO<sub>2</sub>. Meanwhile, the integration of MnO<sub>2</sub> helps enhance the capacitance and current density with better electron transfer of the Ag-MWCNT conductive network. The authors further evaluated the effects of the printed layer numbers on the device performance and revealed a negative correlation between the electrical resistance and the number of printed-layers (**Fig. 6a**). Sundriyal and Bhattacharya<sup>56</sup> presented asymmetric SC electrodes on A4 papers through inkjet printing 40 layers of conducting GO ink on the paper surface. The anode was fabricated through depositing GO-MnO<sub>2</sub> nanocomposite on the substrate; the cathode was made with deposited AC ink. Polyvinyl alcohol (PVA)-LiCl gel was used as the electrolyte. The devices showed outstanding mechanical flexibility and electrochemical performance, holding promise for future low-cost, flexible energy storage applications. The authors found that with the increased layer numbers, the electric charge density would increase for both GO-MnO<sub>2</sub> and AC electrodes (**Fig. 6b**). A comparison between GO-MnO<sub>2</sub> and MnO<sub>2</sub> electrodes were provided, and the incorporation of the GO enhanced the capacitance of the nanocomposite, compare to MnO<sub>2</sub> alone, as shown in **Fig. 6c**.

## 6. Challenges and opportunities

Inkjet printing is a customizable, scalable, waste-free, and lean additive manufacturing process, which can enable seamless device fabrication and integration. Inkjet printing holds promises for scalable manufacturing of integrated, flexible electronic systems that consist of electronic components, sensors, energy units, and interconnects. However, the scientific nature of inkjet printing for nanomanufacturing wearable EES remains elusive, particularly on the ink formulation, substrate effect, spatial resolution, and sintering, which directly impact the productivity, yield, performance uniformity, and batch-to-batch reproducibility. More efforts are required to address the knowledge and technology gaps, at the material, device, and process

levels, in the R&D status quo for inkjet printing of wearable EES. These challenges could be tackled through exploring and understanding the related process-structure-property-functionality relations. Such knowledge will enable the modeling, design, manufacturing, integration, and optimization of the inkjet printing process as an economically-viable option for future scalable nanomanufacturing of wearable EES and various other societally-pervasive technologies.

At the material level, the performance of EES largely depends on the electrode and electrolyte materials, which should be future explored particularly for the inkjet printing process since the performance of these printed devices is still less superior compared to traditional EES. More efforts are needed for exploring non-traditional active materials that are compatible with the inkjet printing, such as  $V_2O_5$  and  $MoO_2$  for SCs, as well as  $LiNiMnCoO_2$  and lithium manganese (LiMn) for LIBs. The emerging materials such as  $PV_2Mo_{10}$ ,  $PMo_{12}$ , Cu-CAT,  $Ti_3C_2T_x$ , VN,  $Fe_2N$ , and TiN, also provide new opportunities for research<sup>55</sup>. Among the list of these emerging materials,  $Ti_3C_2T_x$  has been mostly investigated due to its high metallic conductivity, ion intercalation capability, and the surface hydrophilicity<sup>81, 83, 140, 141</sup>. A very recent study by Zhang *et al.* developed an additive-free 2D titanium carbide ( $Ti_3C_2T_x$ ) MXene ink for MSC via inkjet printing and extrusion printing<sup>82</sup> (**Fig. 6d**). The printed  $Ti_3C_2T_x$  MSC devices showed excellent performance metrics such as excellent retention rate (100% after 10,000 cycles and 97% after 14,000 cycles, respectively). Active materials should be carefully chosen, and the integration of different active materials could be effective in enhancing the electrical performance of the electrodes. The concentration of the electrolyte also impacts the device performance<sup>118</sup>. The incorporation of solvents and surfactant can avoid particle agglomeration and mitigate the coffee-ring effect<sup>107</sup>. The safety issues of the relevant electrolyte and active materials during the device operation should also be considered particularly for future wearable applications such as smart textile, biomedical, and implantable electronics<sup>11</sup>. For instance, acidic electrolyte materials have been widely used for printing flexible EES devices, and they could cause significant issues if there is a leakage in the packaging. Many studies had explored alternative electrolyte materials for SCs, such as organic electrolyte or ionic liquid electrolyte, which not only give rise to superior device performance but also offer reduced toxicity compared to the traditional acidic electrolyte. Besides electrolyte, many widely used surfactants, e.g., DMF and NMP, for dispersing the nanomaterials during inkjet printing are also toxic<sup>94</sup>. More efforts are required to explore and identify appropriate surfactant alternatives that are less or even non-toxic. Last but not least, active materials and electrolytes with inherent flexibility or even stretchability are of significant interests for the wearable EES applications<sup>142-144</sup>.

At the device level, the reported inkjet-printed flexible EES were dominant with the planar and sandwiched device configurations. More intriguing EES configurations such as 3D convoluted structures should be considered and implemented particularly for applications, e.g., smart textile. The self-cleaning and anti-fouling capability of the printed EES is another desired characteristics for the smart textile and implantable applications. Also, it would be desirable to integrate the advantages of both batteries and SCs for implementing flexible EES that possess simultaneously high energy and power densities with other characteristics such as fast charging rate, lightweight, excellent cycling stability, and long lifetime. New device concepts for EES could bring in unprecedented capabilities that transform the energy storage devices into other functional

products, e.g., piezoelectric SCs, photo-SCs, shape-memory SCs, microbial SCs, electrochromic SCs, and self-healing SCs<sup>55</sup>. Cai *et al.* also presented a study on the multifunctional smart window, where the anode and the cathode were fabricated via inkjet printing, and the device can be used as an electrochromic window and an energy storage unit<sup>145</sup>.

At the process level, a holistic process flow that integrates the unit processing modules, e.g., ink formulation, inkjet printing process, annealing, quality evaluation, and packaging, should be designed and standardized for specific EES applications. Standardization of the process can be challenging for inkjet printing of nanomaterial. Hyun *et al.* carried out efforts to explore the feasibility of inkjet printing for scalable manufacturing of EES with high yield and good uniformity (**Fig. 6e**)<sup>70</sup>. The preparation and formulation of the designer functional inks can be potentially scale-up given the versatility in materials synthesis. During the printing, additional energy input such as laser and UV light could be integrated in-line to provide new functionalities of the printed structures<sup>146</sup>. The post-printing annealing of the print film can also be scaled up with the utilization of larger heating plates or other annealing techniques, such as chemical or photonic annealing process<sup>16</sup> (**Fig. 6f**). Compared to the traditional annealing methods, photonic annealing using light sources ranging from infrared<sup>147</sup>, UV<sup>148</sup>, laser<sup>16, 149</sup>, and intense pulsed light<sup>70, 150</sup> could mitigate substrate damage due to excessive heating in the traditional methods, and makes possible the processing of flexible substrates that usually could not withstand the high temperature seen in the traditional annealing process. Further, photonic annealing enables rapid processing and treatment of the defects in the inkjet-printed films for improved electrical performance. More efforts are required, though, to better understand the light-matter interaction during the photonic annealing and its impacts on the active materials in the EES. Processing modules for in-line inspection should be designed and integrated so that real-time structural quality control is possible<sup>151</sup>. Cracking of the printed film with mechanical deformation poses a significant failure mode for flexible EES applications. The incorporation of self-healing materials and structures into the EES presents a promising solution to address the cracking issue. Huang *et al.*<sup>152</sup> demonstrated a self-healing SC capable of stretching over 3,700 % without the occurrence of a crack in the printed film. The material utilized was VSNPs-PAA, which is vinyl hybrid silica nanoparticles crosslinking into PAA chain. In another study, Wang *et al.*<sup>153</sup> reported a manufacturing process for printing shape-memory polymer (SMP) composite using spray deposition followed by a hot-pressing process, which serves as both the annealing and compressing for the printed film to mitigate potential cracking. Last but not least, most reported studies only adopted the inkjet printing process for fabricating one of the device components, primarily the electrodes. To make possible future integrated manufacturing of fully printed flexible EES, more efforts are required for the material and process innovations<sup>124, 125</sup>.

At the application level, the primary concerns are the mechanical stability, package leakage, and cycle stability. Wearable devices tend to be subjected to constant bending and deformation, which demands excellent mechanical stability of the devices. Another potential issue when implementing these devices is the leakage of the packaging since many devices utilized acidic solution as the electrolyte. However, this issue could be potentially addressed with organic electrolyte and ionic liquid electrolyte as replacements.

## 7. Summary and Outlook

The flexible EES has emerged as not only a research topic of interests but also an area of far-reaching societal impacts. The economical manufacturing and integration of flexible EES with controlled properties and desired performance will provide significant opportunities in implementing novel wearable technologies that can operate sustainably. Among all the demonstrated approaches to fabricating EES, as have been reviewed in the previous sections, inkjet printing emerges as a potential economic method for nanomanufacturing wearable EES, due to its energy saving, cost-effectiveness, low working temperature, feasibility for scale-up production, and the potential for printing multifunctional materials into structures with controlled dimensions at designed locations. In order to realize the manufacturing and production potential of inkjet printed flexible EES, more efforts are required to reveal and identify the scientific nature of inkjet printing process for the hierarchical levels of materials, structures, and components in flexible EES, particularly on the ink formulation, ink-substrate interaction, spatial resolution of the printed pattern, post-printing annealing process, and process integration, which directly impact the production rate, yield, performance uniformity, and batch-to-batch reproducibility for future practical production and application of wearable EES. Further, the holistic hybridization of next-generation flexible EES with energy harvesting technologies<sup>154-157</sup> is expected to usher in exciting opportunities in self-powered micro-/nano-systems that can scavenge and store the environmental energy through sustainable pathways. The rapid and exciting progress achieved in many emerging and “traditional” disciplines, e.g., nanomanufacturing, data science, material science, solid-state chemistry, and etc, are expected to excite a confluence of collective efforts from the research community and lead to more theoretical and experimental advances that would ultimately enable the scalable nanomanufacturing of inkjet printed wearable EES (**Fig. 8**).

**Acknowledgments** W. Z. W. acknowledges the College of Engineering and School of Industrial Engineering at Purdue University for the startup support and the Ravi and Eleanor Talwar Rising Star Assistant Professorship. W. Z. W. was partially supported by the National Science Foundation under grant CMMI-1762698.

**Competing financial interest:** The authors declare no competing financial interests.

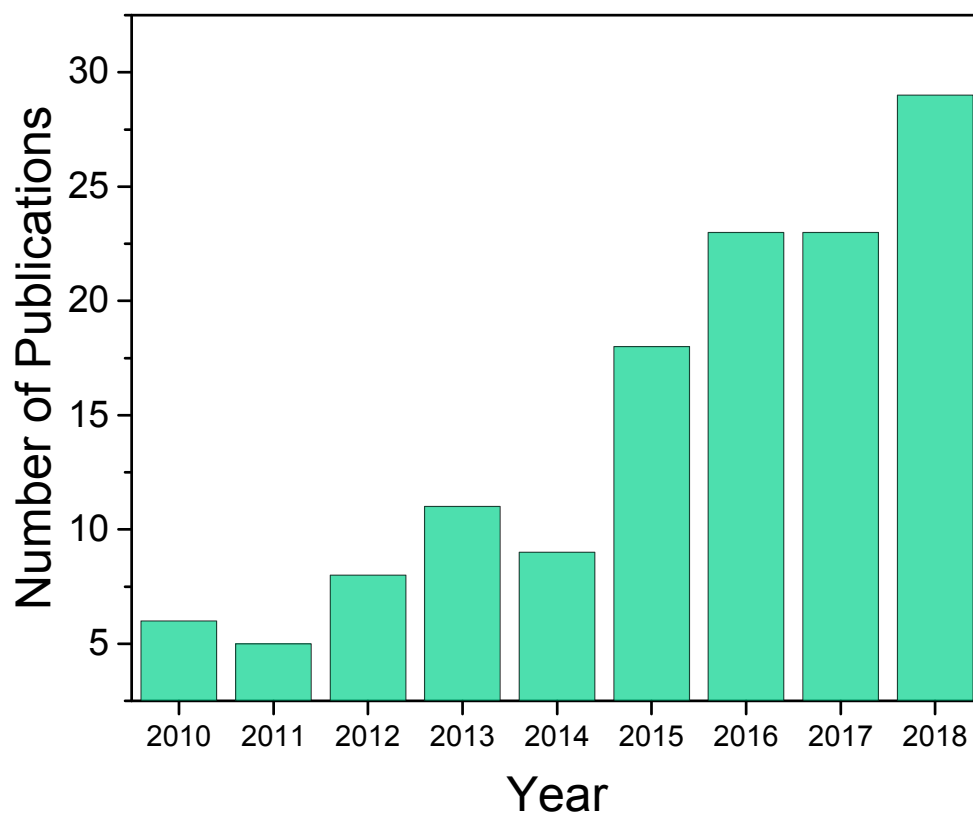


**Figure 1.** The increased interests of the research topic on the inkjet printing of flexible nanomaterials based energy storage devices in recent years.

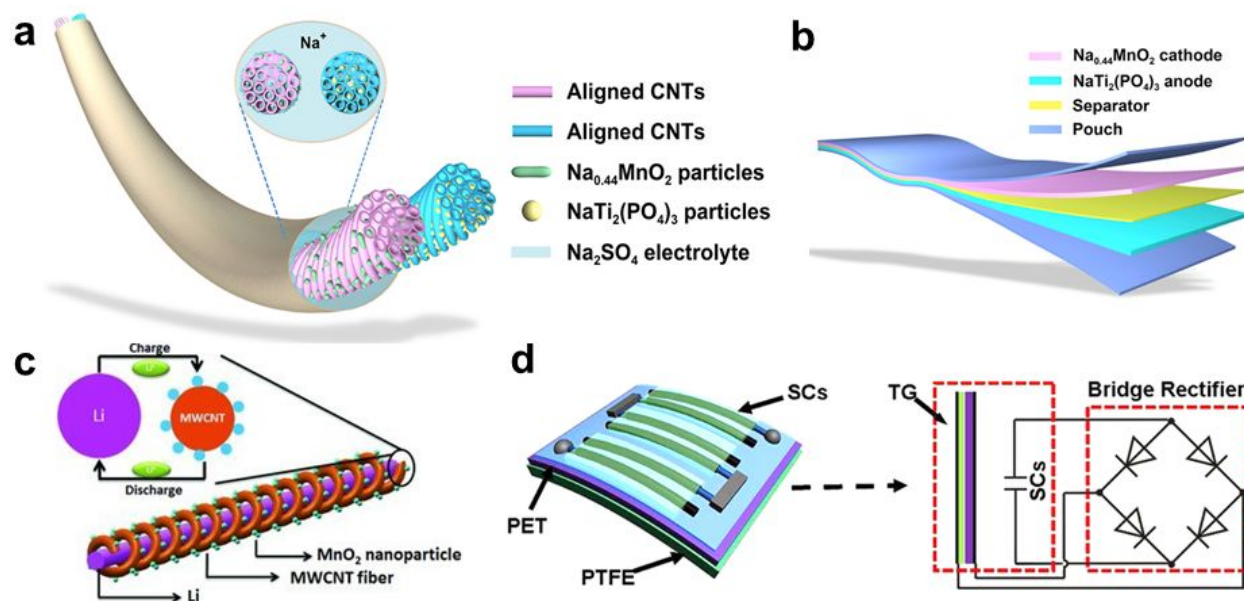


**Figure 2.** **a)** Structure of a cable-type sodium-ion battery<sup>41</sup>. Reproduced with permission. Copyright 2017, Elsevier; **b)** Structure of a sandwich type sodium-ion battery. Reproduced with permission<sup>41</sup>. Copyright 2017, Elsevier; **c)** structure of a wire-shaped lithium-ion battery<sup>85</sup>. Reproduced with permission. Copyright 2013, Wiley-VCH; **d)** Structure of fiber-shaped supercapacitor<sup>86</sup>. Reproduced with permission. Copyright 2019, American Chemical Society.

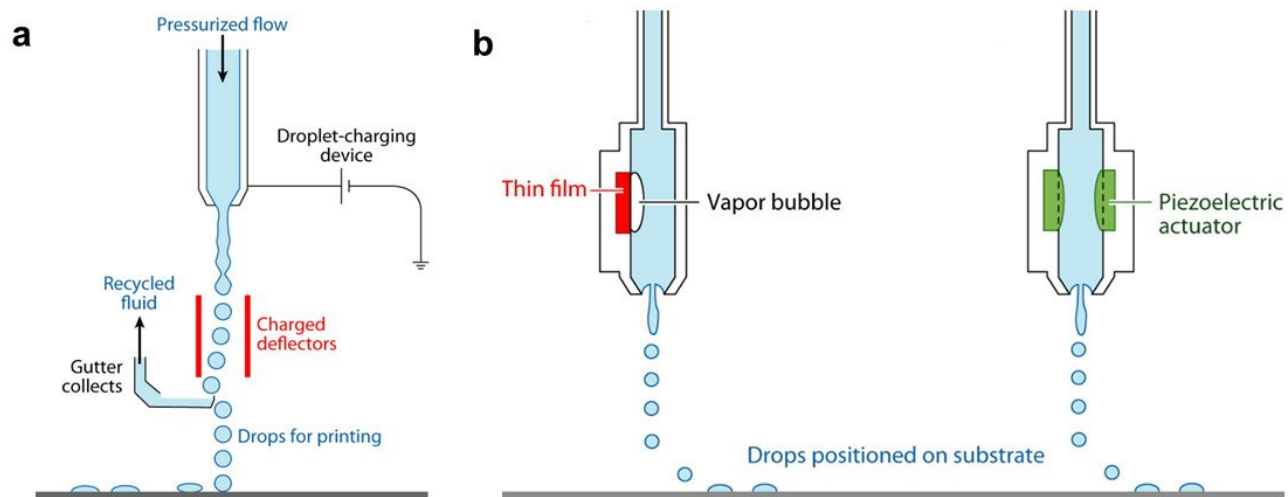


**Figure 3.** Schematic of **a)** Continuous inkjet (CIJ) printer<sup>97</sup>. Reproduced with permission. Copyright 2010, Annual Review of Materials Research; **b)** Drop on demand (DOD) inkjet printer with thermal (left) and piezoelectric (right) printheads<sup>97</sup>. Reproduced with permission. Copyright 2010, Annual Review of Materials Research.

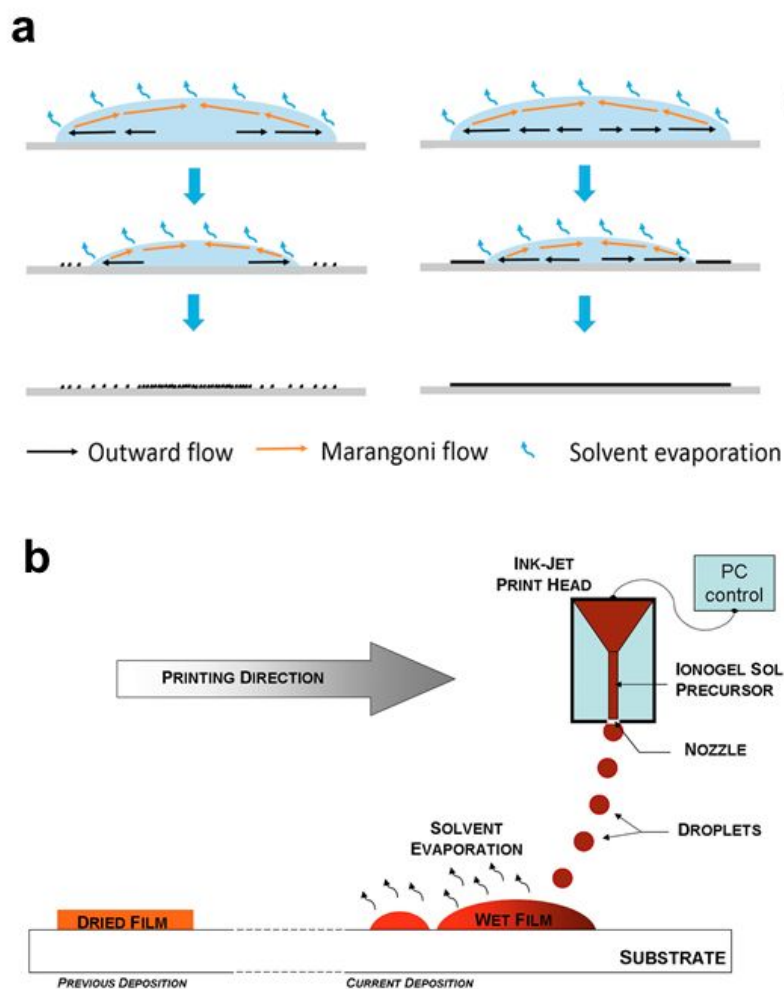


**Figure 4.** **a**) Schematic of the evaporation of the droplet (Marangoni effect)<sup>107</sup>. Reproduced with permission. Copyright 2018, Elsevier; **b**) Schematic of the inkjet printing process for ionogel<sup>116</sup>. Reproduced with permission. Copyright 2015, Elsevier.

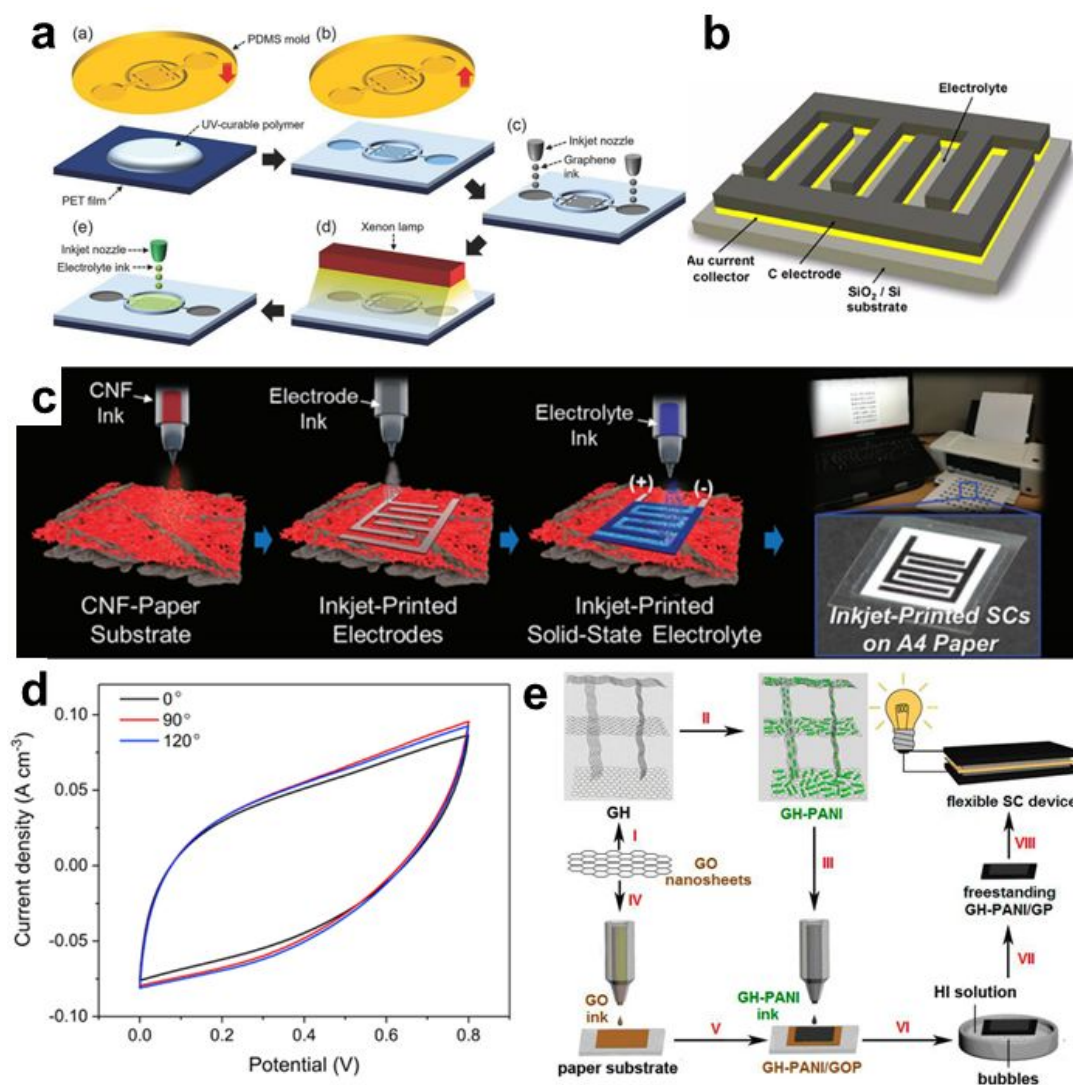


**Figure 5.** **a)** Illustration of an entire fabrication process demonstrated by Hyun et al. for graphene MSC<sup>70</sup>. Reproduced with permission. Copyright 2017, Wiley-VCH; **b)** Schematic of an interdigital micro-supercapacitor<sup>122</sup>. Reproduced with permission. Copyright 2010, Elsevier; **c)** Schematic illustration of a fully inkjet-printed SCs<sup>124</sup>. Reproduced with permission. Copyright 2016, The Royal Society of Chemistry; **d)** CV curve of the MSC under different bending angles at a scan rate of 20 mV s<sup>-1</sup>. Reproduced with permission<sup>107</sup>. Copyright 2018, Elsevier; **e)** Illustration of a fully inkjet-printed GH-PANI supercapacitor. Reproduced with permission<sup>125</sup>. Copyright 2014, American Chemical Society.

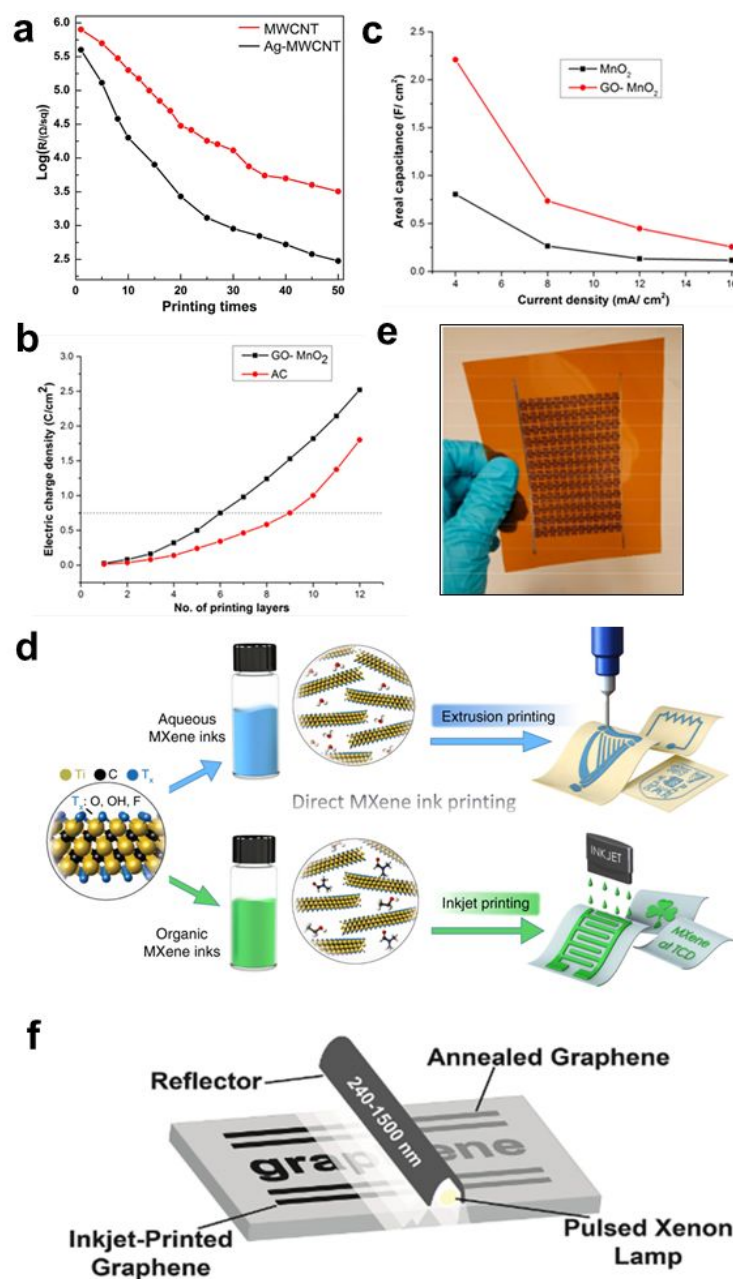


**Figure 6.** **a)** The effect of the number printed layers on the electrical resistance of the devices. Reproduced with permission<sup>108</sup>. Copyright 2015, The Royal Society of Chemistry; **b)** The effect of the number printed layers on the electric of the charge density of the devices. Reproduced with permission<sup>56</sup>. Copyright 2017, American Chemical Society; **c)** Incorporation of GO into MnO<sub>2</sub> leads to higher capacitance. Reproduced with permission<sup>56</sup>. Copyright 2017, American Chemical Society; **d)** Illustration of inkjet printing and extrusion printing of titanium carbide as a supercapacitor fabrication method. Reproduced with permission<sup>82</sup>. Copyright 2019, Nature; **e)** Large-scale of fully inkjet printed MSC<sup>135</sup>. Reproduced with permission. Copyright 2017, American Chemical Society; **f)** Intense pulse lighting setup for annealing graphene inkjet-printed film. Reproduced with permission<sup>150</sup>. Copyright 2015, Wiley-VCH.

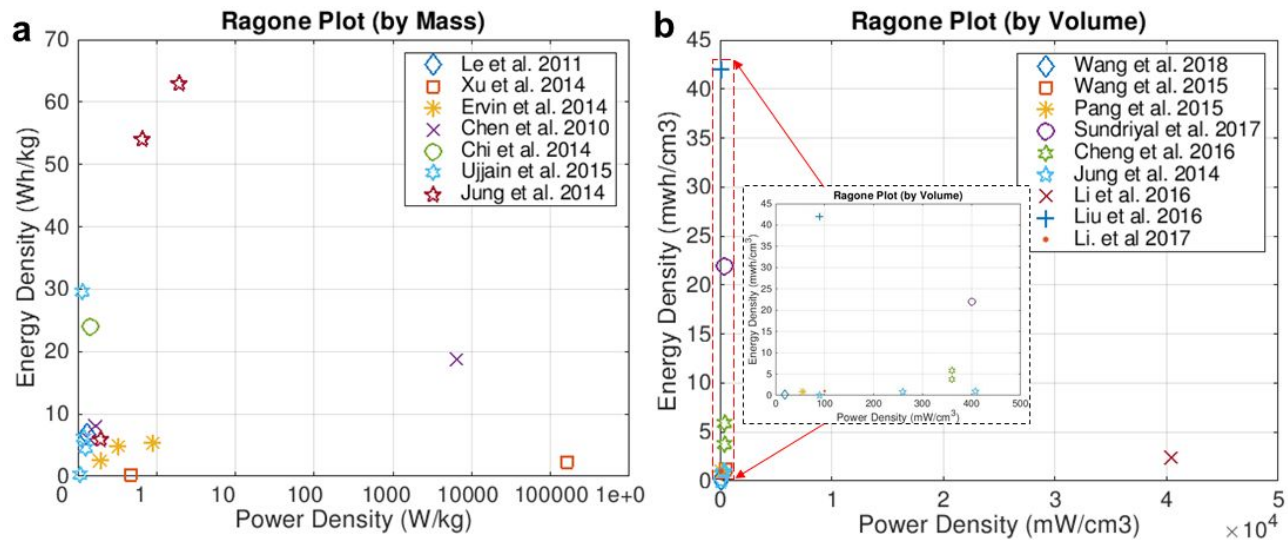


**Figure 7. a)** Ragone plot of flexible energy storage devices fabricated via inkjet printing (per unit mass). Data is compiled from references <sup>118, 119, 121, 123, 125, 130, 131</sup>; **b)** Ragone plot of flexible energy storage devices fabricated via inkjet printing (per unit volume). Data is compiled from references<sup>56, 61, 108, 120, 127, 131, 133-135</sup>.

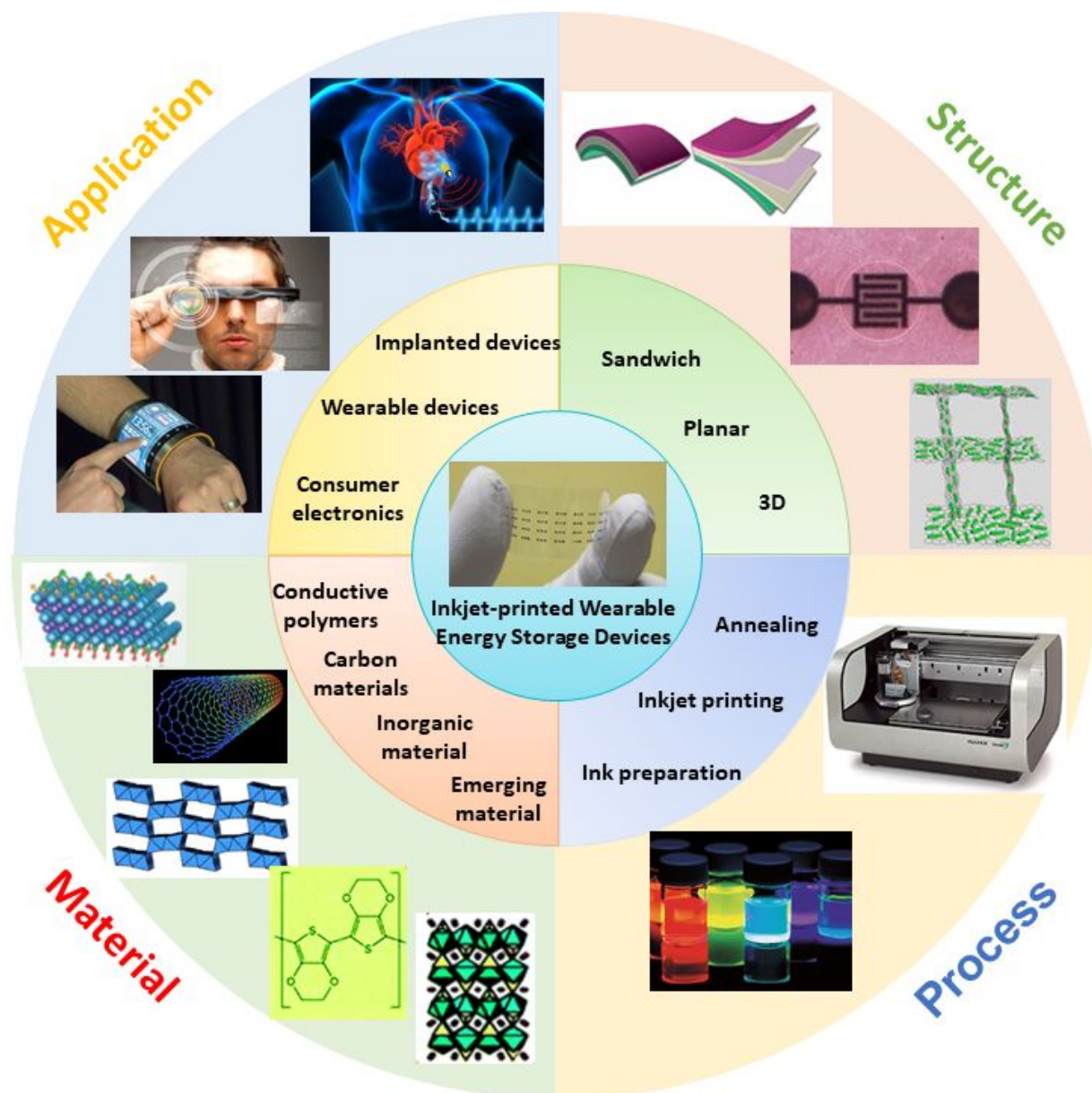


**Figure 8.** The prospect and research opportunities of inkjet printing for the scalable nanomanufacturing of future wearable energy storage devices. Cited in a counterclockwise order taken from Credit: Islam Mosa/University of Connecticut and Maher El-Kady/UCLA; [www.iot-now.com](http://www.iot-now.com); [www.flexenable.com](http://www.flexenable.com); refs <sup>141</sup>; <sup>158</sup>; [www.sackel.com](http://www.sackel.com); [www.fujifilmusa.com](http://www.fujifilmusa.com); refs <sup>125</sup>; <sup>70</sup>; <sup>159</sup>.

## References

1. Z. L. Wang and W. Wu, *Angewandte Chemie-International Edition*, 2012, **51**, 11700-11721.
2. Q. Zheng, Y. Zou, Y. Zhang, Z. Liu, B. Shi, X. Wang, Y. Jin, H. Ouyang, Z. Li and Z. L. Wang, *Science advances*, 2016, **2**, e1501478.
3. J. A. Rogers, T. Someya and Y. Huang, *science*, 2010, **327**, 1603-1607.
4. Y. Liu, M. Pharr and G. A. Salvatore, *ACS Nano*, 2017, **11**, 9614-9635.
5. N. A. Kyeremateng, T. Brousse and D. Pech, *Nature Nanotechnology*, 2016, **12**, 7.
6. D. Dickey Michael, *Advanced Materials*, 2017, **29**, 1606425.
7. X. Pu, M. Liu, X. Chen, J. Sun, C. Du, Y. Zhang, J. Zhai, W. Hu and Z. L. Wang, *Science Advances*, 2017, **3**, e1700015.
8. W. Liu, M.-S. Song, B. Kong and Y. Cui, *Advanced Materials*, 2017, **29**, 1603436.
9. J. Xiong, P. Cui, X. Chen, J. Wang, K. Parida, M.-F. Lin and P. S. Lee, *Nature Communications*, 2018, **9**, 4280.
10. T. Someya, Z. Bao and G. G. Malliaras, *Nature*, 2016, **540**, 379.
11. J. Ren, Q. Xu and Y.-G. Li, *Flexible and Printed Electronics*, 2018, **3**, 013001.
12. L. Li, Z. Lou, D. Chen, K. Jiang, W. Han and G. Shen, *Small*, 2018, **14**, 1702829.
13. D. McManus, S. Vranic, F. Withers, V. Sanchez-Romaguera, M. Macucci, H. Yang, R. Sorrentino, K. Parvez, S.-K. Son, G. Iannaccone, K. Kostarelos, G. Fiori and C. Casiraghi, *Nature Nanotechnology*, 2017, **12**, 343.
14. P. Calvert, *Chemistry of Materials*, 2001, **13**, 3299-3305.
15. M. Gao, L. Li and Y. Song, *Journal of Materials Chemistry C*, 2017, **5**, 2971-2993.
16. S. Wünscher, R. Abbel, J. Perelaer and U. S. Schubert, *Journal of Materials Chemistry C*, 2014, **2**, 10232-10261.
17. N. C. Raut and K. Al-Shamery, *Journal of Materials Chemistry C*, 2018, **6**, 1618-1641.
18. A. Izumi, M. Sanada, K. Furuichi, K. Teraki, T. Matsuda, K. Hiramatsu, H. Munakata and K. Kanamura, *Electrochimica Acta*, 2012, **79**, 218-222.
19. Y. Gu, A. Wu, H. Sohn, C. Nicoletti, Z. Iqbal and J. F. Federici, *Journal of Manufacturing Processes*, 2015, **20**, 198-205.
20. I. Ben-Barak, Y. Kamir, S. Menkin, M. Goor, I. Shekhtman, T. Ripenbein, E. Galun, D. Golodnitsky and E. Peled, *Journal of The Electrochemical Society*, 2019, **166**, A5059-A5064.
21. B. Liu, J. Zhang, X. Wang, G. Chen, D. Chen, C. Zhou and G. Shen, *Nano Letters*, 2012, **12**, 3005-3011.
22. G. Zhou, F. Li and H.-M. Cheng, *Energy & Environmental Science*, 2014, **7**, 1307-1338.
23. L. Nyholm, G. Nyström, A. Mihranyan and M. Strømme, *Advanced Materials*, 2011, **23**, 3751-3769.
24. H. Gwon, H.-S. Kim, K. U. Lee, D.-H. Seo, Y. C. Park, Y.-S. Lee, B. T. Ahn and K. Kang, *Energy & Environmental Science*, 2011, **4**, 1277-1283.
25. S. Li, X. Meng, Q. Yi, J. A. Alonso, M. T. Fernández-Díaz, C. Sun and Z. L. Wang, *Nano Energy*, 2018, **52**, 510-516.
26. H. Lee, S. Kim, K.-B. Kim and J.-W. Choi, *Nano Energy*, 2018, **53**, 225-231.
27. J. Park, M. Park, G. Nam, J.-s. Lee and J. Cho, *Advanced Materials*, 2015, **27**, 1396-1401.

28. Y. Xu, Y. Zhang, Z. Guo, J. Ren, Y. Wang and H. Peng, *Angewandte Chemie International Edition*, 2015, **54**, 15390-15394.
29. C.-Y. Su, H. Cheng, W. Li, Z.-Q. Liu, N. Li, Z. Hou, F.-Q. Bai, H.-X. Zhang and T.-Y. Ma, *Advanced Energy Materials*, 2017, **7**, 1602420.
30. Q. Liu, Y. Wang, L. Dai and J. Yao, *Advanced Materials*, 2016, **28**, 3000-3006.
31. M. Yu, Z. Wang, C. Hou, Z. Wang, C. Liang, C. Zhao, Y. Tong, X. Lu and S. Yang, *Advanced Materials*, 2017, **29**, 1602868.
32. D. Liu, B. Wang, H. Li, S. Huang, M. Liu, J. Wang, Q. Wang, J. Zhang and Y. Zhao, *Nano Energy*, 2019, **58**, 277-283.
33. X. Fan, J. Liu, Z. Song, X. Han, Y. Deng, C. Zhong and W. Hu, *Nano Energy*, 2019, **56**, 454-462.
34. C. A. Milroy, S. Jang, T. Fujimori, A. Dodabalapur and A. Manthiram, *Small*, 2017, **13**, 1603786.
35. X. Fang, W. Weng, J. Ren and H. Peng, *Advanced Materials*, 2016, **28**, 491-496.
36. L. Ma, W. Zhang, L. Wang, Y. Hu, G. Zhu, Y. Wang, R. Chen, T. Chen, Z. Tie, J. Liu and Z. Jin, *ACS Nano*, 2018, **12**, 4868-4876.
37. Y. He, B. Matthews, J. Wang, L. Song, X. Wang and G. Wu, *Journal of Materials Chemistry A*, 2018, **6**, 735-753.
38. N. Song, Z. Gao, Y. Zhang and X. Li, *Nano Energy*, 2019, **58**, 30-39.
39. Q. Liu, Z. Chang, Z. Li and X. Zhang, *Small Methods*, 2018, **2**, 1700231.
40. P. Tan, B. Chen, H. Xu, H. Zhang, W. Cai, M. Ni, M. Liu and Z. Shao, *Energy & Environmental Science*, 2017, **10**, 2056-2080.
41. Z. Guo, Y. Zhao, Y. Ding, X. Dong, L. Chen, J. Cao, C. Wang, Y. Xia, H. Peng and Y. Wang, *Chem*, 2017, **3**, 348-362.
42. F. Bu, P. Xiao, J. Chen, M. F. Aly Aboud, I. Shakir and Y. Xu, *Journal of Materials Chemistry A*, 2018, **6**, 6414-6421.
43. D. Xu, D. Chao, H. Wang, Y. Gong, R. Wang, B. He, X. Hu and H. J. Fan, *Advanced Energy Materials*, 2018, **8**, 1702769.
44. M. Mao, C. Cui, M. Wu, M. Zhang, T. Gao, X. Fan, J. Chen, T. Wang, J. Ma and C. Wang, *Nano Energy*, 2018, **45**, 346-352.
45. H. Yin, H.-Q. Qu, Z. Liu, R.-Z. Jiang, C. Li and M.-Q. Zhu, *Nano Energy*, 2019, **58**, 715-723.
46. Q. Yang, S. Cui, Y. Ge, Z. Tang, Z. Liu, H. Li, N. Li, H. Zhang, J. Liang and C. Zhi, *Nano Energy*, 2018, **50**, 623-631.
47. Y. Ma, A. Sumboja, W. Zang, S. Yin, S. Wang, S. J. Pennycook, Z. Kou, Z. Liu, X. Li and J. Wang, *ACS Applied Materials & Interfaces*, 2019, **11**, 1988-1995.
48. Y. Liu, Z. Sun, K. Tan, D. K. Denis, J. Sun, L. Liang, L. Hou and C. Yuan, *Journal of Materials Chemistry A*, 2019, **7**, 4353-4382.
49. Z. Wu, Y. Wang, X. Liu, C. Lv, Y. Li, D. Wei and Z. Liu, *Advanced Materials*, 2019, **31**, 1800716.
50. D. Chen, Z. Lou, K. Jiang and G. Shen, *Advanced Functional Materials*, 2018, **28**, 1805596.
51. H. Cha, J. Kim, Y. Lee, J. Cho and M. Park, *Small*, 2018, **14**, 1702989.
52. G. Wang, L. Zhang and J. Zhang, *Chemical Society Reviews*, 2012, **41**, 797-828.
53. M. Winter and R. J. Brodd, *Chemical Reviews*, 2004, **104**, 4245-4270.
54. S. Chandra Sekhar, G. Nagaraju and J. S. Yu, *Nano Energy*, 2018, **48**, 81-92.

55. D. P. Dubal, N. R. Chodankar, D.-H. Kim and P. Gomez-Romero, *Chemical Society Reviews*, 2018, **47**, 2065-2129.
56. P. Sundriyal and S. Bhattacharya, *ACS Applied Materials & Interfaces*, 2017, **9**, 38507-38521.
57. Q. Li, Y. Chen, J. Zhang, W. Tian, L. Wang, Z. Ren, X. Ren, X. Li, B. Gao, X. Peng, P. K. Chu and K. Huo, *Nano Energy*, 2018, **51**, 128-136.
58. A. A. Ensafi, S. E. Moosavifard, B. Rezaei and S. K. Kaverlavani, *Journal of Materials Chemistry A*, 2018, **6**, 10497-10506.
59. A. Elmouwahidi, E. Bailón-García, J. Castelo-Quibén, A. F. Pérez-Cadenas, F. J. Maldonado-Hódar and F. Carrasco-Marín, *Journal of Materials Chemistry A*, 2018, **6**, 633-644.
60. J. Hao, S. Peng, H. Li, S. Dang, T. Qin, Y. Wen, J. Huang, F. Ma, D. Gao, F. Li and G. Cao, *Journal of Materials Chemistry A*, 2018, **6**, 16094-16100.
61. Z. Wang, J. Cheng, Q. Guan, H. Huang, Y. Li, J. Zhou, W. Ni, B. Wang, S. He and H. Peng, *Nano Energy*, 2018, **45**, 210-219.
62. Y. Zhu, N. Li, T. Lv, Y. Yao, H. Peng, J. Shi, S. Cao and T. Chen, *Journal of Materials Chemistry A*, 2018, **6**, 941-947.
63. J. Zhan, S. Deng, Y. Zhong, Y. Wang, X. Wang, Y. Yu, X. Xia and J. Tu, *Nano Energy*, 2018, **44**, 265-271.
64. L. Qin, Q. Tao, A. El Ghazaly, J. Fernandez-Rodriguez, P. O. Å. Persson, J. Rosen and F. Zhang, *Advanced Functional Materials*, 2018, **28**, 1703808.
65. X.-X. Li, X.-H. Deng, Q.-J. Li, S. Huang, K. Xiao, Z.-Q. Liu and Y. Tong, *Electrochimica Acta*, 2018, **264**, 46-52.
66. T. Yao, Y. Li, D. Liu, Y. Gu, S. Qin, X. Guo, H. Guo, Y. Ding, Q. Liu, Q. Chen, J. Li and D. He, *Journal of Power Sources*, 2018, **379**, 167-173.
67. R. T. Ginting, M. M. Ovhal and J.-W. Kang, *Nano Energy*, 2018, **53**, 650-657.
68. C. Li, Q. Zhang, S. E, T. Li, Z. Zhu, B. He, Z. Zhou, P. Man, Q. Li and Y. Yao, *Journal of Materials Chemistry A*, 2019, **7**, 2034-2040.
69. Y. Lee, J.-K. Yoo, Y. Oh, H. Park, W. Go, S.-T. Myung and J. Kim, *Journal of Materials Chemistry A*, 2018, **6**, 17571-17578.
70. W. J. Hyun, E. B. Secor, C.-H. Kim, M. C. Hersam, L. F. Francis and C. D. Frisbie, *Advanced Energy Materials*, 2017, **7**, 1700285.
71. P. Geng, S. Zheng, H. Tang, R. Zhu, L. Zhang, S. Cao, H. Xue and H. Pang, *Advanced Energy Materials*, 2018, **8**, 1703259.
72. G. Wang, J. Zhang, S. Yang, F. Wang, X. Zhuang, K. Müllen and X. Feng, *Advanced Energy Materials*, 2018, **8**, 1702254.
73. P. Li, Z. Jin, L. Peng, F. Zhao, D. Xiao, Y. Jin and G. Yu, *Advanced Materials*, 2018, **30**, 1800124.
74. V. Strauss, K. Marsh, M. D. Kowal, M. El-Kady and R. B. Kaner, *Advanced Materials*, 2018, **30**, 1704449.
75. B. Kirubasankar, V. Murugadoss, J. Lin, T. Ding, M. Dong, H. Liu, J. Zhang, T. Li, N. Wang, Z. Guo and S. Angaiah, *Nanoscale*, 2018, **10**, 20414-20425.
76. B. Zhao, L. Zhang, Q. Zhang, D. Chen, Y. Cheng, X. Deng, Y. Chen, R. Murphy, X. Xiong, B. Song, C.-P. Wong, M.-S. Wang and M. Liu, *Advanced Energy Materials*, 2018, **8**, 1702247.

77. L. Manjakkal, C. G. Núñez, W. Dang and R. Dahiya, *Nano Energy*, 2018, **51**, 604-612.
78. C. Qu, L. Zhang, W. Meng, Z. Liang, B. Zhu, D. Dang, S. Dai, B. Zhao, H. Tabassum, S. Gao, H. Zhang, W. Guo, R. Zhao, X. Huang, M. Liu and R. Zou, *Journal of Materials Chemistry A*, 2018, **6**, 4003-4012.
79. F. Yu, Z. Chang, X. Yuan, F. Wang, Y. Zhu, L. Fu, Y. Chen, H. Wang, Y. Wu and W. Li, *Journal of Materials Chemistry A*, 2018, **6**, 5856-5861.
80. J. Azadmanjiri, V. K. Srivastava, P. Kumar, M. Nikzad, J. Wang and A. Yu, *Journal of Materials Chemistry A*, 2018, **6**, 702-734.
81. M. R. Lukatskaya, S. Kota, Z. Lin, M.-Q. Zhao, N. Shpigel, M. D. Levi, J. Halim, P.-L. Taberna, M. W. Barsoum, P. Simon and Y. Gogotsi, *Nature Energy*, 2017, **2**, 17105.
82. C. Zhang, L. McKeon, M. P. Kremer, S.-H. Park, O. Ronan, A. Seral-Ascaso, S. Barwich, C. Ó. Coileáin, N. McEvoy, H. C. Nerl, B. Anasori, J. N. Coleman, Y. Gogotsi and V. Nicolosi, *Nature Communications*, 2019, **10**, 1795.
83. H. Li and J. Liang, *Advanced Materials*, 2019, **0**, 1805864.
84. J. Luo, C. Fang, C. Jin, H. Yuan, O. Sheng, R. Fang, W. Zhang, H. Huang, Y. Gan, Y. Xia, C. Liang, J. Zhang, W. Li and X. Tao, *Journal of Materials Chemistry A*, 2018, **6**, 7794-7806.
85. J. Ren, L. Li, C. Chen, X. Chen, Z. Cai, L. Qiu, Y. Wang, X. Zhu and H. Peng, *Advanced Materials*, 2013, **25**, 1155-1159.
86. X. Xiao, T. Li, P. Yang, Y. Gao, H. Jin, W. Ni, W. Zhan, X. Zhang, Y. Cao, J. Zhong, L. Gong, W.-C. Yen, W. Mai, J. Chen, K. Huo, Y.-L. Chueh, Z. L. Wang and J. Zhou, *ACS Nano*, 2012, **6**, 9200-9206.
87. Y. Wang, Q. Yang, Y. Zhao, S. Du and C. Zhi, *Advanced Materials Technologies*, 2019, **0**, 1900083.
88. M. Beidaghi and C. Wang, *Advanced Functional Materials*, 2012, **22**, 4501-4510.
89. J. H. Kim, K.-W. Nam, S. B. Ma and K. B. Kim, *Carbon*, 2006, **44**, 1963-1968.
90. V. O. Khavrus, M. Weiser, M. Fritsch, R. Ummethala, M. G. Salviaggio, M. Schneider, M. Kusnezoff and A. Leonhardt, *Chemical Vapor Deposition*, 2012, **18**, 53-60.
91. J. Jiang, J. Liu, W. Zhou, J. Zhu, X. Huang, X. Qi, H. Zhang and T. Yu, *Energy & Environmental Science*, 2011, **4**, 5000-5007.
92. Y. S. Yoon, W. I. Cho, J. H. Lim and D. J. Choi, *Journal of Power Sources*, 2001, **101**, 126-129.
93. C. Zhu, T. Liu, F. Qian, W. Chen, S. Chandrasekaran, B. Yao, Y. Song, E. B. Duoss, J. D. Kuntz, C. M. Spadaccini, M. A. Worsley and Y. Li, *Nano Today*, 2017, **15**, 107-120.
94. S. Lawes, A. Riese, Q. Sun, N. Cheng and X. Sun, *Carbon*, 2015, **92**, 150-176.
95. Z. Li, Q. Yang, K. Fan, W. Xie, W. Qiao, M. Shao and M. Wei, *Journal of Materials Chemistry A*, 2018, **6**, 21287-21294.
96. J. Wang, Q. Sun, X. Gao, C. Wang, W. Li, F. B. Holness, M. Zheng, R. Li, A. D. Price, X. Sun, T.-K. Sham and X. Sun, *ACS Applied Materials & Interfaces*, 2018, **10**, 39794-39801.
97. B. Derby, *Annual Review of Materials Research*, 2010, **40**, 395-414.
98. C. C. Ho, K. Murata, D. A. Steingart, J. W. Evans and P. K. Wright, *Journal of Micromechanics and Microengineering*, 2009, **19**, 094013.
99. J. Chang, J. He, Q. Lei and D. Li, *ACS Applied Materials & Interfaces*, 2018, **10**, 19116-19122.

100. Q. Lei, J. He, B. Zhang, J. Chang and D. Li, *Journal of Materials Chemistry C*, 2018, **6**, 213-218.
101. J. Li, F. Ye, S. Vaziri, M. Muhammed, M. C. Lemme and M. Östling, *Advanced Materials*, 2013, **25**, 3985-3992.
102. M. Michel, J. A. Desai, C. Biswas and A. B. Kaul, *Nanotechnology*, 2016, **27**, 485602.
103. G. Hu, J. Kang, L. W. T. Ng, X. Zhu, R. C. T. Howe, C. G. Jones, M. C. Hersam and T. Hasan, *Chemical Society Reviews*, 2018, **47**, 3265-3300.
104. S. K. Garlapati, M. Divya, B. Breitung, R. Kruk, H. Hahn and S. Dasgupta, *Advanced Materials*, 2018, **30**, 1707600.
105. T. Juntunen, H. Jussila, M. Ruoho, S. Liu, G. Hu, T. Albrow-Owen, L. W. T. Ng, R. C. T. Howe, T. Hasan, Z. Sun and I. Tittonen, *Advanced Functional Materials*, 2018, **28**, 1800480.
106. S. Chung, K. Cho and T. Lee, *Advanced Science*, 2019, **6**, 1801445.
107. Y. Wang, Y.-Z. Zhang, D. Dubbink and J. E. ten Elshof, *Nano Energy*, 2018, **49**, 481-488.
108. S. Wang, N. Liu, J. Tao, C. Yang, W. Liu, Y. Shi, Y. Wang, J. Su, L. Li and Y. Gao, *Journal of Materials Chemistry A*, 2015, **3**, 2407-2413.
109. P. Chang, H. Mei, S. Zhou, K. G. Dassios and L. Cheng, *Journal of Materials Chemistry A*, 2019, **7**, 4230-4258.
110. M. Hilder, B. Winther-Jensen and N. B. Clark, *Journal of Power Sources*, 2009, **194**, 1135-1141.
111. W. Yuan, Y. Zhang, L. Cheng, H. Wu, L. Zheng and D. Zhao, *Journal of Materials Chemistry A*, 2016, **4**, 8932-8951.
112. P. E. Delannoy, B. Riou, T. Brousse, J. Le Bideau, D. Guyomard and B. Lestriez, *Journal of Power Sources*, 2015, **287**, 261-268.
113. J. Huang, J. Yang, W. Li, W. Cai and Z. Jiang, *Thin Solid Films*, 2008, **516**, 3314-3319.
114. Y. Zhao, Q. Zhou, L. Liu, J. Xu, M. Yan and Z. Jiang, *Electrochimica Acta*, 2006, **51**, 2639-2645.
115. Y. Zhao, G. Liu, L. Liu and Z. Jiang, *JOURNAL OF SOLID STATE ELECTROCHEMISTRY*, 2009, **13**, 705-711.
116. P. E. Delannoy, B. Riou, B. Lestriez, D. Guyomard, T. Brousse and J. Le Bideau, *Journal of Power Sources*, 2015, **274**, 1085-1090.
117. F. Xu, T. Wang, W. Li and Z. Jiang, *Chemical Physics Letters*, 2003, **375**, 247-251.
118. M. H. Ervin, L. T. Le and W. Y. Lee, *Electrochimica Acta*, 2014, **147**, 610-616.
119. L. T. Le, M. H. Ervin, H. Qiu, B. E. Fuchs and W. Y. Lee, *Electrochemistry Communications*, 2011, **13**, 355-358.
120. H. Pang, Y. Zhang, W.-Y. Lai, Z. Hu and W. Huang, *Nano Energy*, 2015, **15**, 303-312.
121. P. Chen, H. Chen, J. Qiu and C. Zhou, *Nano Research*, 2010, **3**, 594-603.
122. D. Pech, M. Brunet, P.-L. Taberna, P. Simon, N. Fabre, F. Mesnilgrete, V. Conédéra and H. Durou, *Journal of Power Sources*, 2010, **195**, 1266-1269.
123. Y. Xu, I. Hennig, D. Freyberg, A. James Strudwick, M. Georg Schwab, T. Weitz and K. Chih-Pei Cha, *Journal of Power Sources*, 2014, **248**, 483-488.
124. K.-H. Choi, J. Yoo, C. K. Lee and S.-Y. Lee, *Energy & Environmental Science*, 2016, **9**, 2812-2821.

125. K. Chi, Z. Zhang, J. Xi, Y. Huang, F. Xiao, S. Wang and Y. Liu, *ACS Applied Materials & Interfaces*, 2014, **6**, 16312-16319.
126. Z. Liu, Z.-S. Wu, S. Yang, R. Dong, X. Feng and K. Müllen, *Advanced Materials*, 2016, **28**, 2217-2222.
127. T. Cheng, Y.-Z. Zhang, J.-P. Yi, L. Yang, J.-D. Zhang, W.-Y. Lai and W. Huang, *Journal of Materials Chemistry A*, 2016, **4**, 13754-13763.
128. A. Chiolerio, S. Bocchini and S. Porro, *Advanced Functional Materials*, 2014, **24**, 3375-3383.
129. S. Sollami Delekta, A. D. Smith, J. Li and M. Östling, *Nanoscale*, 2017, **9**, 6998-7005.
130. S. K. Ujjain, R. Bhatia, P. Ahuja and P. Attri, *PLOS ONE*, 2015, **10**, e0131475.
131. H. Jung, C. Ve Cheah, N. Jeong and J. Lee, *Applied Physics Letters*, 2014, **105**, 053902.
132. P. Zhibin, H. Haibo, L. Guojin and Y. Changhui, *Nano-Micro Letters*, 2017, **9**.
133. L. Li, E. B. Secor, K.-S. Chen, J. Zhu, X. Liu, T. Z. Gao, J.-W. T. Seo, Y. Zhao and M. C. Hersam, *Advanced Energy Materials*, 2016, **6**, 1600909.
134. W. Liu, C. Lu, H. Li, R. Y. Tay, L. Sun, X. Wang, W. L. Chow, X. Wang, B. K. Tay, Z. Chen, J. Yan, K. Feng, G. Lui, R. Tjandra, L. Rasenthiram, G. Chiu and A. Yu, *Journal of Materials Chemistry A*, 2016, **4**, 3754-3764.
135. J. Li, S. Sollami Delekta, P. Zhang, S. Yang, M. R. Lohe, X. Zhuang, X. Feng and M. Östling, *ACS Nano*, 2017, **11**, 8249-8256.
136. F. Zhang, M. Wei, V. V. Viswanathan, B. Swart, Y. Shao, G. Wu and C. Zhou, *Nano Energy*, 2017, **40**, 418-431.
137. V. Augustyn, P. Simon and B. Dunn, *Energy & Environmental Science*, 2014, **7**, 1597-1614.
138. K. V. Sankar, S. C. Lee, Y. Seo, C. Ray, S. Liu, A. Kundu and S. C. Jun, *Journal of Power Sources*, 2018, **373**, 211-219.
139. H. Wang, M. Wang and Y. Tang, *Energy Storage Materials*, 2018, **13**, 1-7.
140. M. R. Lukatskaya, S.-M. Bak, X. Yu, X.-Q. Yang, M. W. Barsoum and Y. Gogotsi, *Advanced Energy Materials*, 2015, **5**, 1500589.
141. C. Zhang, M. P. Kremer, A. Seral-Ascaso, S.-H. Park, N. McEvoy, B. Anasori, Y. Gogotsi and V. Nicolosi, *Advanced Functional Materials*, 2018, **28**, 1705506.
142. Y. Wang, C. Zhu, R. Pfattner, H. Yan, L. Jin, S. Chen, F. Molina-Lopez, F. Lissel, J. Liu, N. I. Rabiah, Z. Chen, J. W. Chung, C. Linder, M. F. Toney, B. Murmann and Z. Bao, *Science Advances*, 2017, **3**, e1602076.
143. J. Y. Oh, S. Rondeau-Gagné, Y.-C. Chiu, A. Chortos, F. Lissel, G.-J. N. Wang, B. C. Schroeder, T. Kurosawa, J. Lopez, T. Katsumata, J. Xu, C. Zhu, X. Gu, W.-G. Bae, Y. Kim, L. Jin, J. W. Chung, J. B. H. Tok and Z. Bao, *Nature*, 2016, **539**, 411.
144. M. Vatankhah-Varnosfaderani, W. F. M. Daniel, M. H. Everhart, A. A. Pandya, H. Liang, K. Matyjaszewski, A. V. Dobrynin and S. S. Sheiko, *Nature*, 2017, **549**, 497.
145. G. Cai, P. Darmawan, X. Cheng and P. S. Lee, *Advanced Energy Materials*, 2017, **7**, 1602598.
146. S. Jin, Y. Wang, M. Motlag, S. Gao, J. Xu, Q. Nian, W. Wu and G. J. Cheng, *Advanced Materials*, 2018, **30**.
147. H.-J. Hwang, K.-H. Oh and H.-S. Kim, *Scientific Reports*, 2016, **6**, 19696.

148. J. Troughton, M. J. Carnie, M. L. Davies, C. Charbonneau, E. H. Jewell, D. A. Worsley and T. M. Watson, *Journal of Materials Chemistry A*, 2016, **4**, 3471-3476.
149. M. A. Skylar-Scott, S. Gunasekaran and J. A. Lewis, *Proceedings of the National Academy of Sciences*, 2016, **113**, 6137.
150. E. B. Secor, B. Y. Ahn, T. Z. Gao, J. A. Lewis and M. C. Hersam, *Advanced Materials*, 2015, **27**, 6683-6688.
151. S. Zhang, *Optics and Lasers in Engineering*, 2018, **106**, 119-131.
152. Y. Huang, M. Zhong, Y. Huang, M. Zhu, Z. Pei, Z. Wang, Q. Xue, X. Xie and C. Zhi, *Nature Communications*, 2015, **6**, 10310.
153. X. Wang, J. Sparkman and J. Gou, *Composites Science and Technology*, 2017, **141**, 8-15.
154. C. Ma, S. Gao, X. Gao, M. Wu, R. Wang, Y. Wang, Z. Tang, F. Fan, W. Wu, H. Wan and W. Wu, *InfoMat*, 2019, **1**, 116-125.
155. Y. Wang, R. Wang, S. Wan, Q. Wang, M. J. Kim, D. Ding and W. Wu, *Nano Futures*, 2019, **3**, 011001.
156. S. Gao, R. Wang, C. Ma, Z. Chen, Y. Wang, M. Wu, Z. Tang, N. Bao, D. Ding, W. Wu, F. Fan and W. Wu, *Journal of Materials Chemistry A*, 2019.
157. R. Wang, S. Gao, Z. Yang, Y. Li, W. Chen, B. Wu and W. Wu, *Advanced Materials*, 2018, **30**.
158. D. P. Dubal, O. Ayyad, V. Ruiz and P. Gómez-Romero, *Chemical Society Reviews*, 2015, **44**, 1777-1790.
159. N. Yu, M.-Q. Zhu and D. Chen, *Journal of Materials Chemistry A*, 2015, **3**, 7910-7918.